Atmospheric
Chemistry
and Physics
Discussions
Open Access
EGU

1 OH and HO₂ radical chemistry in a midlatitude forest: Measurements and

2 model comparisons

3 Michelle M. Lew[1*], Pamela S. Rickly[2**], Brandon P. Bottorff[1], Sofia Sklaveniti[2,3], Thierry Léonardis[3],
4 Nadine Locoge[3], Sebastien Dusanter[3], Shuvashish Kundu[4***], Ezra Wood[5], and Philip S. Stevens[1,2]

5 [1] Department of Chemistry, Indiana University, Bloomington, IN 47405, USA
6 [2] O'Neill School of Public and Environmental Affairs, Indiana University, Bloomington, IN 47405, USA
7 [3] IMT Lille Douai, Univ. Lille, SAGE – Département Sciences de l'Atmosphère et Génie de l'Environnement, 59000 Lille,
8 France
9 [4] Department of Chemistry, University of Massachusetts - Amherst, Amherst, MA 01003, USA
10 [5] Department of Chemistry, Drexel University, Philadelphia, PA 19104, USA

11 * now at California Air Resources Board, Sacramento, CA 95812, USA
12 ** now at Cooperative Institute for Research in Environmental Sciences, University of Colorado, Boulder, CO 80309, USA
13 and Chemical Sciences Division, Earth System Research Laboratory, National Oceanic and Atmospheric Administration,
14 Boulder, CO 80305, USA
15 *** now at Momentive Performance Materials, Inc., Tarrytown, NY 10591, United States

16 *Correspondence*: Philip S. Stevens (pstevens@indiana.edu)

17 **Abstract.** Reactions of the hydroxyl (OH) and peroxy radicals (HO₂ and RO₂) play a central role in the chemistry of the

18 atmosphere. In addition to controlling the lifetimes of many trace gases important to issues of global climate change, OH

19 radical reactions initiate the oxidation of volatile organic compounds (VOCs) which can lead to the production of ozone and

20 secondary organic aerosols in the atmosphere. Previous measurements of these radicals in forest environments characterized

21 by high mixing ratios of isoprene and low mixing ratios of nitrogen oxides (NO₍ₓ₎) have shown serious discrepancies with

22 modeled concentrations. These results bring into question our understanding of the atmospheric chemistry of isoprene and

23 other biogenic VOCs under low NO₍ₓ₎ conditions.

24 During the summer of 2015, OH and HO₂ radical concentrations as well as total OH reactivity were measured using

25 Laser-Induced Fluorescence - Fluorescence Assay by Gas Expansion (LIF-FAGE) techniques as part of the Indiana Radical,

26 Reactivity and Ozone Production Intercomparison (IRRONIC). This campaign took place in a forested area near the Indiana

27 University, Bloomington campus characterized by high mixing ratios of isoprene and low mixing ratios of NO₍ₓ₎. Supporting

28 measurements of photolysis rates, VOCs, NO₍ₓ₎, and other species were used to constrain a zero-dimensional box model based

29 on the Regional Atmospheric Chemistry Mechanism (RACM2) and the Master Chemical Mechanism (MCM). Using an OH

30 chemical scavenger technique, the study revealed the presence of an interference with the LIF-FAGE measurements of OH

31 that increased with both ambient concentrations of ozone and temperature. Subtraction of the interference resulted in measured

32 OH concentrations that were in better agreement with model predictions, although the model still underestimated the measured

33 concentrations, likely due to an underestimation of the concentration of NO at this site. Measurements of HO₂ radical

1 concentrations during the campaign included a fraction of isoprene-based peroxy radicals ($HO_2^*=HO_2 + \alpha RO_2$) and were

2 found to agree with model predictions. On average, the measured reactivity was consistent with that calculated from measured

3 OH sinks to within 20%, with modeled oxidation products accounting for the missing reactivity, although significant missing

4 reactivity (approximately 40% of the total measured reactivity) was observed on some days.

5 1 Introduction

6 The hydroxyl radical (OH) is one of the primary oxidants in the atmosphere (Levy, 1972). The OH radical initiates the

7 oxidation of volatile organic compounds (VOCs) that leads to the production of hydroperoxy radicals (HO_2) and organic

8 peroxy radicals (RO_2). In the presence of nitrogen oxides ($NO_x = NO + NO_2$), reactions of these radicals can lead to the

9 production of ozone and secondary organic aerosols in the atmosphere, the primary components of photochemical smog.

10 Because of their short atmospheric lifetimes, measurements of OH and HO_2 (together HO_x) and total OH reactivity can provide

11 a robust test of our understanding of this complex chemistry (Heard and Pilling, 2003).

12 Multiple field campaigns have been conducted over the years measuring OH and HO_2 radicals in both urban and

13 forested environments. Measurements of OH in urban areas characterized by high mixing ratios of NO_x and anthropogenic

14 VOCs have been generally consistent with model predictions (Ren et al., 2003; Shirley et al., 2006; Kanaya et al., 2007a;

15 Dusanter et al., 2009b; Hofzumahaus et al., 2009; Griffith et al., 2016), while measurements in remote forested environments

16 characterized by low mixing ratios of NO_x and high mixing ratios of biogenic VOCs have often been greater than model

17 predictions (Tan et al., 2001; Lelieveld et al., 2008; Whalley et al., 2011; Rohrer et al., 2014).

18 However, recent measurements by Mao et al. (2012) in a northern California forest using a new chemical scavenging

19 technique that removes ambient OH before air enters the detection cell revealed a significant interference associated with their

20 Laser-Induced Fluorescence (LIF) measurements of OH. The unknown interference was a factor of 2 to 3 times higher than

21 ambient OH concentrations (Mao et al., 2012). Similar results were observed in a boreal forest by Novelli et al. (2014), who

22 observed an interference using a similar chemical scrubbing technique that was a factor of 3 to 4 times higher than ambient

23 OH concentrations. One possible source of this observed interference may be the decomposition of Criegee intermediates

24 produced from the ozonolysis of biogenic emissions in the low-pressure detection cells used by LIF instruments, although the

25 ambient concentration of these intermediates in the atmosphere may be too low to explain all of the observed interference

26 (Novelli et al., 2017; Rickly and Stevens, 2018). Another proposed source of the interference is the decomposition of ROOOH

27 molecules inside the FAGE detection cell formed from the reaction of OH with RO_2 radicals (Fittschen et al., 2019).

28 Nevertheless, interferences associated with measurements of OH could explain part of the discrepancies between measured

29 and modeled OH concentrations in forested environments. Monitoring potential interferences associated with OH

30 measurements using LIF techniques may be crucial for understanding the discrepancies between measurements and models.

31 In contrast to measurements of OH, the agreement between measured and modeled HO_2 concentrations have been

32 highly variable. In urban environments, measured HO_2 concentrations were sometimes found to agree with model predictions

1 (Shirley et al., 2006; Emmerson et al., 2007; Dusanter et al., 2009b; Michoud et al., 2012; Lu et al., 2013; Ren et al., 2013;

2 Griffith et al., 2016), while other times the measurements were found to be both lower (George et al., 1999; Konrad et al.,

3 2003) and higher than model predictions (Martinez et al., 2003; Ren et al., 2003; Emmerson et al., 2005; Kanaya et al., 2007a;

4 Chen et al., 2010; Sheehy et al., 2010; Czader et al., 2013; Griffith et al., 2016). In forested environments, measured HO_2

5 concentrations were sometimes found to agree with model predictions (Tan, D. et al., 2001; Ren et al., 2005; 2006), but were

6 often found to be either lower (Carslaw et al., 2001; Kanaya et al., 2007b; Whalley et al., 2011; Kanaya et al., 2012; Mao et

7 al., 2012; Griffith et al., 2013), or higher than model predictions (Carslaw et al., 2001; Kubistin et al., 2010; Kim et al., 2013;

8 Hens et al., 2014). Part of this variability may be due to interferences from alkene and aromatic based RO_2 radicals converting

9 to HO_2 in systems that detect HO_2 through conversion to OH by addition of NO in the sample cell. The degree to which the

10 RO_2 species can interfere with HO_2 measurements has been quantified through laboratory experiments (Fuchs et al., 2011;

11 Whalley et al., 2013; Lew et al., 2018). The extent of RO_2 radical contributions during HO_2 measurements in previous

12 campaigns is unclear.

13   Total OH reactivity measurements can complement HO_x measurements by providing a constraint on the total loss of

14 OH that can be compared to that calculated from co-located measurements of OH sinks. Several recent studies have identified

15 discrepancies between measured and calculated OH reactivity in which the measured values are significantly greater than the

16 calculated values (Di Carlo et al., 2004; Hansen et al., 2014; Nölscher et al., 2016; Zannoni et al., 2016). This difference has

17 been attributed to OH loss from unmeasured VOCs and their oxidation products. In general, significant missing OH reactivity

18 has not been observed as often in urban environments as it has in forested areas, bringing into question our understanding of

19 the chemistry of biogenic emissions and their oxidation products (Dusanter and Stevens, 2017).

20   This study reports measurements and model simulations of HO_x radical chemistry as well as OH reactivity for a

21 forested site located in Bloomington, Indiana during the 2015 IRRONIC (Indiana Radical Reactivity and Ozone productioN

22 InterComparison) field campaign. This work compares the measured HO_x radical concentrations to model predictions

23 incorporating the Regional Atmospheric Chemistry Mechanism 2 (RACM2), in addition to a version updated to include the

24 Leuven Isoprene Mechanism (RACM2-LIM1), as well as the Master Chemical Mechanism versions 3.2 and 3.3.1 in order to

25 test the ability of each model to reproduce the observed radical concentrations and total OH reactivity.

26 **2 Experimental section**

27 **2.1 IRRONIC location and supporting measurements**

28 The IRRONIC campaign site was located within a mixed deciduous forest (sugar maple, sycamore, tulip polar, ash and hickory

29 trees) at the Indiana University Research and Teaching Preserve (IU-RTP) field lab (39.1908º N, 86.502º W) located

30 approximately 2.5 km northeast of the center of the Indiana University campus, and 1 km from the IN 45/46 bypass at the

31 northern perimeter. The goals of the campaign included an informal intercomparison of peroxy radical measurements by two

32 different techniques (Kundu et al., 2019), an analysis of ozone production sensitivity at this site (Sklaveniti et al., 2018), a

1 comparison of measured OH radical reactivity with that calculated from measured VOCs, and a comparison of measured OH,

2 HO_2, and RO_2 radicals with model predictions. The main biogenic emission within this area was isoprene, with an average

3 daytime maximum mixing ratio of approximately 4 ppb during the campaign. This area exhibited low anthropogenic influence

4 from the campus area, with an average daytime maximum mixing ratio of NO of approximately 315 ppt and an average day-

5 time maximum NO_2 mixing ratio of approximately 2 ppb. Measurements were conducted on top of two scaffolding platforms

6 adjacent to the field lab, approximately 1.8 m from the ground. Additional information regarding the field site and the

7 IRRONIC campaign can be found in Sklaveniti et al. (2018) and Kundu et al. (2019).

8   Table 1 summarizes the major instrumentation employed during the campaign. NO was measured every 10 s using a

9 chemiluminescence instrument (Thermo model 42i-TL, detection limit 50 ppt / 2 min). Periodic problems with the sensor's

10 high voltage power supply that required an eventual replacement limited the coverage of the measurements. NO_2 was measured

11 every 1 s by a Cavity Attenuated Phase Shift (CAPS) instrument (detection limit 40 ppt / 10 s), and ozone was measured every

12 10 sec using a 2B Technologies model 202 UV absorbance instrument (detection limit 3 ppb / 10 s). Further details on the

13 calibration and baseline measurements for the NO, NO_2, and O_3 measurements are described in Kundu et al. (2019).

14 Nonmethane hydrocarbons, including C2-C10 alkanes and alkenes, butadiene, C6-C9 aromatic compounds, isoprene, α-

15 pinene, and β-pinene, were measured using a thermal desorption GC/FID instrument with a 1.5-h time resolution. Oxygenated

16 VOCs (OVOCs), including C2-C10 aldehydes, C2-C6 ketones, and C2-C4 alcohols, were measured by thermal desorption

17 GC/FID-MS with a 1.5-h time resolution. Offline sampling focused on measurements of oxygenated VOCs including

18 formaldehyde and C2-C6 aldehydes, acetone, MEK, glyoxal and methylglyoxal using DNPH cartridges and HPLC-UV

19 analysis. C6-C16 VOCs including α-pinene, β-pinene, limonene, camphene, heptane-hexadecane, methylpentene-pentadecene

20 were measured using Sorbent cartridges and GC-MS analysis. Measurements of $J(NO_2)$ were made by spectral radiometry

21 courtesy of the University of Houston. HONO was measured using a newly developed Laser Photofragmentation/Laser-

22 Induced Fluorescence instrument (Bottorff et al., 2015; Bottorff et al., in prep).

23 2.2 HO$_x$ radical measurements

24 The Indiana University LIF-FAGE instrument (IU-FAGE) has been described in detail previously (Dusanter et al., 2009a

25 Griffith et al., 2013; 2016). In the LIF-FAGE technique, OH radicals are detected by laser-induced fluorescence after expansion

26 of ambient air to low pressure. This extends the OH fluorescence lifetime, allowing temporal filtering of the fluorescence from

27 laser scatter (Heard and Pilling, 2003). Ambient air is expanded through a 0.64 mm diameter orifice located at the top of a

28 cylindrical nozzle (5 cm in diameter and 20 cm long), resulting in a flow rate of approximately 3 SLPM through the sampling

29 nozzle. Two scroll pumps (Edwards XDS 35i) connected in parallel maintain a pressure inside the cell of 5.5 Torr.

30   The laser system used in this study consisted of a Spectra Physics Navigator II YHP40-532Q that produces

31 approximately 8 W of radiation at 532 nm at a repetition rate of 10 kHz which is used to pump a Sirah Credo Dye laser (255

32 mg/L of Rhodamine 610 and 80 mg/L of Rhodamine 101 in ethanol), resulting in 40 to 100 mW of radiation at 308 nm. After

33 exiting the dye laser, a fraction of the radiation is focused onto the entrance of a 12-m optical fiber to transmit the radiation to

Atmospheric
Chemistry
and Physics
Discussions

1   the sampling cell which was placed on top of the 1.8-m platform adjacent to the field lab. In the detection cell, the laser crosses

2   the expanded air perpendicular to the flow in a White cell configuration with 24 passes. For this campaign, the laser power

3   inside the sampling cell ranged from 0.5 to 4.4 mW and was monitored using a photodiode at the exit of the White cell.

4   OH radicals are excited and detected using the $A^2\Sigma^+$ $\upsilon' = 0 \leftarrow X^2\Pi$ $\upsilon'' = 0$ transition near 308 nm (Stevens et al., 1994).

5   The net signal is measured by spectral modulation by tuning the wavelength on- and off-resonance in successive modulation

6   cycles. A reference cell where OH is produced by thermal dissociation of water vapor is used to ensure that the laser is tuned

7   on and off the OH transition. The OH fluorescence is detected using a microchannel plate photomultiplier tube (MCP-PMT)

8   detector (Hamamatsu R5946U-50), a preamplifier (Stanford Research System SR445) and a gated photon counter (Stanford

9   Research Systems SR 400). The MCP-PMT is switched off during the laser pulse through the use of electronic gating allowing

10   the OH fluorescence to be temporally filtered from laser scattered light. A Teflon injector located approximately 2.5 cm below

11   the inlet and 17.5 cm above the detection axis allowed for the addition of NO (approximately 2 sccm, 1.4×10^{13} cm^{-3}, Matheson

12   Gas, 10% in N_2) to convert ambient HO_2 to OH through the fast $HO_2 + NO \rightarrow OH + NO_2$ reaction, allowing for indirect

13   measurements of HO_2.

14   The IU-FAGE instrument is calibrated by producing known quantities of OH and HO_2 from the photolysis of water

15   vapor in air using a mercury penlamp within the calibration source as described previously (Dusanter et al., 2008). For these

16   calibrations, zero air was sent through a humidifier and delivered at a flow rate of 38-50 L min^{-1} to the calibration source.

17   Uncertainties associated with the UV water photolysis calibration technique have been described previously (Dusanter et al.,

18   2008) and are estimated to be 18% (1σ) for both OH and HO_2.

19   **2.2.1 Measurement of OH interferences**

20   The LIF-FAGE measurements are subject to potential interferences where OH radicals are generated inside the detection cell.

21   For example, ozone can be photolyzed by the laser and in the presence of water vapor can produce hydroxyl radicals (Davis

22   et al., 1981a; 1981b) (reactions R1 and R2):

23   $O_3 + h\upsilon \rightarrow O(^1D) + O_2$ (R1)

24   $O(^1D) + H_2O \rightarrow 2OH$ (R2)

25   This interference in the IU-FAGE instrument is monitored through laboratory calibrations utilizing various concentrations of

26   ozone, water vapor, and laser power. To characterize this and any other interference during ambient measurements, a chemical

27   scrubbing technique is used to remove ambient OH prior to entering the detection cell (Griffith et al., 2016; Rickly and Stevens,

28   2018). This chemical modulation technique is used to monitor levels of the laser-generated ozone-water interference and any

29   other processes that may produce OH radicals within the excitation axis.

30   Hexafluoropropylene (C_3F_6, 95.5% in N_2, Matheson) is added through a circular injector 1 cm above the nozzle with

31   a flow rate of approximately 3.5 sccm to remove 95% of externally generated OH (Rickly and Stevens, 2018). During ambient

32   measurements, chemical addition of C_3F_6 is modulated in between ambient OH measurements every 15 minutes for a duration

33   of 10 minutes. The differences between the measured OH during C_3F_6 addition and OH measurements including the

1   interference represents the net ambient OH concentration in the atmosphere. Taking the measurement of potential interferences

2   into account results in a limit of detection for OH for this campaign of approximately 7.9×10^5 cm^{-3} for a 30 min average (S/N

3   = 1).

4   **2.2.2 Contribution of RO$_2$ interferences during HO$_2$ measurements**

5   As discussed above, HO$_2$ radicals are measured indirectly after sampling ambient air at low pressure through chemical

6   conversion to OH by addition of NO and subsequent detection of OH by LIF:

7        $HO_2 + NO \rightarrow OH + NO_2$ (R3)
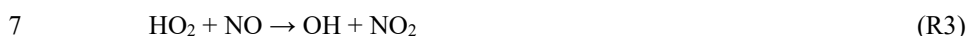
8   It was previously believed that the detection of HO$_2$ radicals using this technique was free from interferences from the reaction

9   of RO$_2$ radicals with NO, as model simulations and measurements suggested that the rate of conversion of RO$_2$ radicals to HO$_2$

10   by reactions R4 and R5 and subsequent conversion to OH through reaction R3 were negligible. This was due to the slow rate

11   of reaction R5 under the reduced oxygen concentration in the low pressure LIF-FAGE cell and the short reaction time between

12   injection of NO and detection of OH (Heard and Pilling, 2003).

13        $RO_2 + NO \rightarrow RO + NO_2$ (R4)

14        $RO + O_2 \rightarrow R'O + HO_2$ (R5)
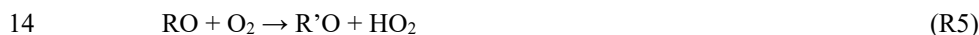
15   For example, RO$_2$ radicals produced from the OH-initiated oxidation of small alkanes were found to produce a negligible yield

16   of HO$_2$ (Stevens et al., 1994; Kanaya et al., 2001; Tan, et al., 2001; Creasey et al., 2002; Holland et al., 2003). However, recent

17   laboratory studies have shown that there are interferences associated with measurements of HO$_2$ from the conversion of RO$_2$

18   radicals derived from the OH-initiated oxidation of alkenes and aromatics to HO$_2$ (and subsequently OH) by reaction with NO.

19   The high conversion efficiency of alkene-based peroxy radicals to HO$_2$ is due to the ability of the β-hydroxyalkoxy radicals

20   produced from OH + VOC reactions to rapidly decompose, forming a hydroxyalkyl radical which then reacts rapidly with O$_2$

21   leading to the production of a carbonyl compound and HO$_2$ (Fuchs et al., 2011; Whalley et al., 2013; Lew et al., 2018). Because

22   of this interference, measurements of peroxy radicals that are sensitive to this interference are denoted as HO$_2$* ([HO$_2$*] =

23   [HO$_2$] + α [RO$_2$], 0<α<1). The conversion efficiency depends on the instrumental characteristics and configurations employed

24   as well as the amount of NO added. The RO$_2$-to-HO$_2$ conversion efficiencies for a number of different peroxy radicals have

25   been characterized for current and past configurations of the IU-FAGE instrument (Lew et al., 2018). For the configuration of

26   the IU-FAGE instrument used in this study, the conversion efficiency of isoprene-based peroxy radicals was found to be

27   approximately 83%, while the conversion efficiency of propane peroxy radicals was found to be approximately 15%. The

28   precision for the HO$_2$* measurement does not depend on the RO$_2$ interference and results in a limit of detection for HO$_2$*

29   during this campaign of 7×10^7 cm^{-3} for a 30 second average (S/N =1).

30

2.3 OH reactivity measurements

The IU Total OH Loss rate Method (TOHLM) instrument is based on the method of Kovacs and Brune (2001) and is described in detail elsewhere (Hansen et al., 2014). Briefly, the instrument is comprised of a flow tube reactor measuring 5 cm in diameter and 75 cm in length. Ambient air is introduced through an 8 cm diameter perfluoroalkoxy polymer film hose attached to the flow tube at a flow rate of approximately 180 SLPM using a regenerative blower (Spencer VB001) to establish turbulent flow conditions. Previous measurements have demonstrated that different lengths of this inlet tubing do not significantly impact the measured OH reactivity (Hansen et al., 2014). A pitot-static tube (Dwyer Instruments) is positioned just before the exit of the flow tube facing the turbulent core of the flow, approximately 1 cm from the flow tube wall. The pitot-static tube is connected to a 0-1 Torr differential pressure gauge (MKS Instruments) to measure the total flow tube velocity.

OH radicals are produced in a movable injector that houses a mercury pen lamp (UV Pen-Ray) in which the top of the pen lamp was positioned at the end of the injector, just before a spiral Teflon spray nozzle used to promote mixing within the flow tube (McMaster Carr). In addition, a turbulizer is attached to the injector tube 24 cm before the spray nozzle consisting of four 1 cm wide fins to promote turbulent flow conditions as well as to provide support of the injector throughout the flow tube. The injector is inserted along the main axis and is configured for automated movement acquiring continuous measurements in the forward and backward directions. A nitrogen flow of 10 standard liters per minute (SLPM) is bubbled through high-purity water (EMD Chemicals) producing water vapor which is directed through the injector and photolyzed by the penlamp to produce OH with typical concentrations on the order of 10^9 cm^{-3}. This method is known to also produce HO_2 radicals, which can lead to a regeneration of OH at NO mixing ratios greater than 1 ppbv (Kovacs and Brune, 2001). However, because the average NO mixing ratio measured over the course of the campaign was below this value, no correction to the measured reactivity was applied (Hansen et al., 2014).

OH radicals were measured using a similar FAGE detection cell described above. Ambient air was expanded through a 1 mm diameter orifice to a total pressure of approximately 6 Torr. OH radicals were excited by a portion of the 308 nm output of the dye laser, with the resulting fluorescence detected by a gated channel photomultiplier tube detector (Excelitas MP 1300) and monitored by a photon counter (Stanford Research SRS 400). A 2 meter long optical fiber was used to transmit the 308-nm laser beam to the OH reactivity detection cell which was located inside the field lab. The laser power was measured at the exit of the detection cell and monitored with a photodiode.

As ambient air entered the flow tube, the automated OH source injector allowed for varying reaction time with the ambient air over a distance of approximately 15 cm for a period of 2.5 minutes. This produced an OH decay over a reaction time of 0-0.15 s from which the OH reactivity was determined. Losses of OH on the walls of the flow tube were measured by flowing high-purity nitrogen (Indiana Oxygen) at 180 SLPM through the flow tube in addition to the OH production through the injector to measure the decay of OH in the absence of any VOCs. Several measurements of this wall loss (k_b) resulted in an average value of 10 ± 2 s^{-1} (1σ).

1   The calculated OH reactivity for a measured compound X (k_X), can be determined from the product of the

2   concentration of X and its second-order rate constant with OH:

3    $$k_X = k_{OH+X}[X] \qquad (1)$$

4   Summation of this value for each reacting species gives the total OH reactivity (k_{OH}):

5    $$k_{OH} = \sum_i k_{OH+X_i}[X_i] \qquad (2)$$

6   Under pseudo-first order conditions ([OH]<<[X]), the OH concentration within the flow tube can be expressed as a first-order

7   exponential decay:

8    $$[OH]_t = [OH]_0 e^{-(k_{OH}+k_b)t} \qquad (3)$$

9   Solving for k_{OH}, the OH reactivity, gives:

10    $$k_{OH} = -\frac{\Delta \ln[OH]}{\Delta t} - k_b \qquad (4)$$

11   Measurements of the change in the concentration of OH over the reaction time produces the measured OH reactivity value.

12   These measurements can be compared to the calculated total reactivity from measured OH sinks (Eq. 2) to determine whether

13   the measured total OH reactivity can be accounted for by the measured sinks. The difference between the measured and

14   calculated total OH reactivity is referred to as the "missing" OH reactivity.

15   Laboratory measurements of the reactivity of several VOCs with well-known rate constants showed that the OH

16   reactivity measurements are on average 30% lower than calculated when the measured velocity of the turbulent core is used

17   to determine the reaction time, likely due to either incomplete mixing of the reactants or a systematic underestimation of the

18   reaction time (Hansen et al, 2014). As a result, the measured ambient OH reactivity values were scaled by a factor of 1.41.

19   Measurements performed over a range of OH reactivity values suggest that the IU-TOHLM instrument can measure OH

20   reactivity up to 45 s^{-1} with a precision (1σ) of 1.2 s^{-1} + 4% of the measured value for a 10 min average (Hansen et al., 2014).

21   **2.4 Modeling HO$_x$ concentrations and OH reactivity**

22   Ambient measurements of OH, HO$_2$*, and total OH reactivity were modeled with the Regional Atmospheric Chemistry

23   Mechanism (RACM2) (Goliff et al., 2013) and the Master Chemical Mechanism version 3.2 (Jenkin et al., 1997; Saunders et

24   al., 2003). The isoprene oxidation mechanism in RACM2 was updated to include the Leuven Isoprene Mechanism (LIM1)

25   originally proposed by Peeters, et al. (2009) involving peroxy radical isomerization reactions leading to additional HO$_x$ radical

26   production (Tan et al., 2017). The addition also includes a revision of the chemistry of first-generation isoprene oxidation

27   products, including methyl vinyl ketone (MVK), methacrolein (MACR), and isoprene hydroperoxides (ISHP) (Tan et al.,

28   2017). In addition, the ambient measurements were also modeled with version 3.3.1 of the Master Chemical Mechanism

1 (MCM). In comparison to MCM 3.2, MCM 3.3.1 includes an updated isoprene oxidation mechanism based on the LIM

2 mechanism resulting in HO_x recycling from peroxy radical H-shift isomerization reactions (Jenkin et al., 2015).

3   The Framework for 0-D Atmospheric Modeling (F0AM) was used to calculate the radical concentrations and OH

4 reactivity observed at the IRRONIC site (Wolfe et al., 2016). The model was constrained by the 30 minute average measured

5 mixing ratios of ozone, NO_x, and VOCs and processed through a 5 day spin-up to generate unmeasured secondary oxidation

6 products. Table S1 summarizes the measured compounds and includes their grouping into the condensed RACM2 model

7 inputs. Because the VOC measurements occurred every 90 minutes, the measurements were interpolated into 30 min bins

8 before input to the model. Due to the minimal overlap of the NO measurements with the HO_x measurements, the model was

9 constrained to the measured diurnal averaged mixing ratio of NO for all days. The measured $J(NO_2)$ was used to scale the

10 model calculated $J(NO_2)$ and other photolysis rates. The model uncertainty is approximately 30% (1σ), estimated from

11 uncertainties associated with the input parameters and the rate constants for each reaction (Griffith et al., 2013; Wolfe et al.,

12 2016).

3 Results and discussion

14 Campaign diurnal average measurements of $J(NO_2)$, temperature, isoprene, O_3, NO_2, and NO are summarized in Fig. 1. The

15 maximum average mixing ratio of NO of approximately 315 ppt was observed at approximately 08:00 (EDT), while the

16 average mixing ratio of NO_2 reached a maximum of 2 ppb around 10:00. Average mixing ratios of isoprene ranged from 0.4

17 to 4.4 ppb, reaching a maximum around 18:00. Anthropogenic VOCs were relatively low at this site, with maximum mixing

18 ratios of benzene less than 80 ppt. Day-to-day profiles (July 10 to July 25) are illustrated in Fig. 2, showing measurements of

19 O_3, temperature, isoprene, NO_x, HO_2*, and OH. Unfortunately, instrumental problems limited the NO measurements prior to

20 19 July.

3.1 OH measurements and model comparison

22 OH concentrations were determined using the chemical modulation technique described above using external C_3F_6 addition to

23 scavenge ambient OH and measure interferences producing OH inside the IU-FAGE detection cell, including laser generated

24 OH. The measured interferences were subtracted from the total OH signal determined from spectral modulation, resulting in

25 net ambient OH concentrations (Fig. 2). As can be seen from this figure, the measured interference was a significant fraction

26 of the total OH signal on many days. On average the measured interference (including laser-generated OH from equations R1

27 and R2) accounted for approximately 50% of the total signal during the day (08:00-20:00) and as much as 100% of the signal

28 at night.

29   Figure 3 illustrates the total measured OH radical signal by spectral modulation (black circles), the measured

30 interference (blue squares), and the expected laser-generated interference from reactions 3 and 4 calculated from laboratory

31 calibrations (Griffith et al., 2016) (green points) during 14 July and 15 July. On 15 July, the measured interference was similar

1 to the calculated interference suggesting that the majority of the measured interference was laser-generated. However, on 14

2 July, the measured interference was much larger than the calculated interference, suggesting that the majority of the measured

3 interference was due to an unknown source. Subtraction of the calculated laser-generated interference from the measured

4 interference on all days resulted in a measurement of the unknown interference that increased with both ozone and temperature

5 during the campaign (Fig. 4).

6 This result is consistent with the observations from Mao et al. (2012) who found that the interference measured in

7 their LIF-FAGE instrument using a similar chemical modulation technique increased with ozone and total OH reactivity. The

8 observed increase in the magnitude of the unknown interference with ozone and temperature suggests that the interference

9 may be related to the ozonolysis of biogenic VOCs, whose emissions increase with temperature. Previous measurements have

10 shown that some LIF-FAGE instruments, including the IU-FAGE instrument, are susceptible to an interference under high

11 concentrations of ozone and biogenic VOCs, perhaps due to the decomposition of Criegee intermediates inside the FAGE

12 detection cell (Fuchs et al., 2016; Novelli et al., 2017; Rickly and Stevens, 2018). However, estimated concentrations of

13 Criegee intermediates in similar environments on the order of 5×10^4 cm^{-3} (Novelli et al., 2017) are too low to explain the

14 observed interference during the IRRONIC campaign.

15 The observation of a significant interference during this campaign is in contrast to previous measurements of OH by

16 the IU-FAGE instrument in a forested environment during the CABINEX 2009 campaign (Griffth et al., 2013). During this

17 campaign, several tests were conducted where C_3F_6 or CO was added to remove ambient OH. These tests did not reveal any

18 significant interference, and measurements of OH were found to be in good agreement with model predictions (Griffith et al.,

19 2013). One possible explanation for this discrepancy with the measurements during IRRONIC is the lower levels of ozone and

20 temperatures observed during CABINEX compared to IRRONIC. Average mixing ratios of ozone during CABINEX were

21 near 30 ppb and average temperatures were near 20°C during the day, with average mixing ratios of isoprene less than 2 ppb

22 in the afternoon. These levels of ozone and temperature are lower than that where the interference was observed during

23 IRRONIC (Fig. 4), suggesting that a similar interference was likely undetectable during CABINEX.

24 Recent measurements have found that NO_3 radicals can lead to an interference in FAGE instruments (Fuchs et al.,

25 2016), although the mechanism for production of this interference is not known. Such an interference in the IU-FAGE

26 instrument could explain the observed interference during some nights (Fig. 3), but is unlikely the source of the interference

27 during the daytime. Another possible source of the interference is the decomposition of ROOOH molecules inside the FAGE

28 detection cell formed from the reaction of OH with RO_2 radicals (Fittschen et al., 2019). However, assuming a rate constant

29 of 1×10^{-10} cm^{-3} s^{-1} for the OH + RO_2 reaction, it is unlikely that a significant fraction of RO_2 radicals will react to form

30 ROOOH under the mixing ratios of NO observed at this site, as the estimated lifetime of RO_2 radicals with respect to reaction

31 with NO was an order-of-magnitude shorter than that for reaction with OH. Additional measurements and laboratory tests will

32 be needed to identify and minimize interferences associated with LIF-FAGE measurements of OH.

33 The day-to-day measurements of OH after the interference has been subtracted for 10-20 July and 24-25 July are

34 illustrated in Fig. 5. Measurements on 21-22 July focused on measurements of HO_2^*, thus OH measurements were not

1 conducted on those days. This figure also illustrates the day-to-day model results for OH and HO$_2$* from the base RACM2

2 and the modified RACM2-LIM1 models, as well as the MCM versions 3.2 and 3.3.1, illustrating that, the predicted OH

3 concentrations are generally lower than the measured concentrations for both the RACM2 and MCM models.

4   Figure 6 (top) shows the average diurnal profile of the OH measurements, both with and without the measured

5 interference for the days illustrated in Fig. 5. The average ambient diurnal OH radical concentration reached a maximum of

6 approximately 4-5 × 10^6 cm^{-3} after the measured interference was subtracted. If the measured interference was not subtracted

7 from the total OH signal determined by spectral modulation, the resulting OH radical concentrations would be as high as 9 ×

8 10^6 cm^{-3} (Fig. 6), much greater than the averaged RACM2 and MCM modeled maximum concentrations of approximately 2

9 × 10^6 cm^{-3}. The daytime OH radical concentration measurements after the interference has been subtracted are in better

10 agreement with the model results, but are still approximately a factor of two times larger from 12:00 to midnight and appear

11 to peak later than the model predictions. Including versions of the LIM1 mechanism for HO$_x$ regeneration in both the RACM2

12 model (RACM2-LIM1) and the MCM (MCM 3.3.1) results in somewhat higher modeled daytime concentrations of OH

13 compared to the base RACM2 and MCM 3.2 mechanisms, although the results are still lower than the measured concentrations

14 (Fig. 6). However, as seen in Fig. 6, if the measured interference was not subtracted, OH radical concentrations would be a

15 factor of 4-5 times higher than the model predictions.

16   A possible reason for the model underprediction of the measurements is an underestimation of the concentration of

17 NO in the model. As discussed above, instrumental problems limited the measurements of NO primarily to several days at the

18 end of the campaign, resulting in approximately 3 days that overlapped with the OH measurements (Fig. 2). Consistent

19 measurements were only obtained after replacing the instrument's detector. In order to model the remaining days of the

20 campaign, the model was constrained to the diurnal average of the NO measurements from the latter half of the campaign.

21 However, it is possible that the actual mixing ratio of NO during the early days of the campaign was higher than the average

22 value measured during the end of the campaign, given that the measured NO$_2$ concentrations during the early part of the

23 campaign were approximately a factor of 2 greater than that measured during the latter part of the campaign (20-24 July) (Fig.

24 2). For the days at the end of the campaign where there was significant overlap between the measurements of OH and NO, the

25 model results are in better agreement during these days (20 and 24 July) (Fig. 5). The diurnal average model results are in

26 better agreement with the measurements when mixing ratios of NO were unconstrained while constraining mixing ratios of

27 NO$_2$ and O$_3$. As shown in Fig. 6, unconstraining the concentration of NO in the MCM 3.3.1 model increases the predicted OH

28 concentrations by approximately a factor of 3 during the daytime with model predicted mixing ratios of NO approximately a

29 factor of 2 greater than the constrained values during the day. Although the model still underestimates the measurements of

30 OH in the afternoon, it is clear that without taking the observed OH interference into account, the measured OH concentrations

31 would have been a factor of 5 greater than predicted by the model mechanisms, similar to previous measurements under

32 comparable mixing ratios of isoprene and NO$_x$ (Rhorer et al., 2014).

3.2 HO$_2$* measurements and model comparison

The day-to-day measurements of HO$_2$* are illustrated in Fig. 5 with the RACM2, RACM2-LIM1, MCM 3.2 and MCM 3.3.1 model results. The contribution of modeled RO$_2$ radicals to the modeled HO$_2$* is based on laboratory calibrations of the RO$_2$– to–HO$_2$ conversion efficiencies for the sampling conditions used in this study (Lew et al., 2018) and are incorporated into both versions of the RACM2, and MCM peroxy radical categories. Under the instrumental conditions during the campaign, the conversion efficiency of isoprene-based peroxy radicals to HO$_2$ was determined to be approximately 83 ± 7%, while the conversion efficiency of methyl peroxy radicals was estimated to be approximately 5% (Lew et al., 2018). These two peroxy radicals accounted for the majority of RO$_2$ radicals predicted by the models (see below). The maximum measured HO$_2$* concentration each day during the campaign was generally between approximately 2×10^8 and 2×10^9 molecules cm^{-3} (Figs. 2 and 5), with an average daily maximum value of approximately 1×10^9 cm^{-3} (Fig. 6). The RACM2-LIM1 and MCM 3.3.1 modeled diurnal averaged HO$_2$* reached a maximum of approximately 1.3×10^9 cm^{-3} and 9.5×10^8 cm^{-3}, respectively, compared to a value of 1.2×10^9 cm^{-3} for the RACM2 modeled HO$_2$* and 9.1×10^8 molecules cm^{-3} for the MCM 3.2 modeled HO$_2$* (Fig. 6).

The predicted HO$_2$*concentrations by the base RACM2 model are in good agreement with the measured concentrations, overpredicting the measurements by approximately 20% on average, although the model agrees with the measurements to within the combined uncertainty of the model and the measurements. Including the LIM1 mechanism in the RACM2 mechanism increases the modeled HO$_2$* by approximately 15% due to the modeled increase in HO$_x$ radical production from the isomerization of isoprene-based peroxy radicals. The MCM-based model results are also in good agreement with the measured HO$_2$* although they tend to underpredict the measured concentrations by approximately 20% on average in the afternoon (Fig. 5 and 6). The MCM 3.3.1 mechanism results in predicted HO$_2$* concentrations that are approximately 5% greater than that predicted by MCM 3.2 in the afternoon when NO concentrations are low due to the inclusion of HO$_x$ production from the isomerization of isoprene-based peroxy radicals. These results are also consistent with a possible under-estimation of the actual concentrations of NO at the site as discussed above. Unconstraining the mixing ratio of NO in the MCM 3.3.1 model increases the averaged modeled HO$_2$* concentrations to values similar to that predicted by the RACM2 model, but still within approximately 20% of the measured concentrations and in better agreement with the measurements in the late afternoon (Fig. 6). These results are in contrast to that observed during the CABINEX campaign, where a RACM-based model overpredicted the measured HO$_2$* by as much as a factor of 2 (Griffith et al., 2013), likely related to the higher concentrations of NO observed during IRRONIC compared to CABINEX increasing the importance of the HO$_2$ + NO and RO$_2$ + NO reactions in determining the fate of these radicals.

The MCM 3.2 and MCM 3.3.1 diurnal average modeled HO$_2$* concentrations and the model contribution of peroxy radicals to HO$_2$* are shown in Fig. 7 (left panels). The diurnal profile of the HO$_2$* radical concentration predicted by the MCM models includes contributions primarily from isoprene peroxy radicals and HO$_2$ radicals, with smaller contributions from methyl peroxy and acetyl peroxy radicals (Fig. 7). The RACM2 models produced similar results, with HO$_2$ and isoprene peroxy

1   radicals contributing to the majority of the modeled HO_2^* concentrations (Fig S1). The total modeled RO_x (RO_2 + HO_2)

2   concentrations by the different mechanisms are also shown in Fig. 7 (right panels). The MCM 3.2 model predicted that the

3   diurnal average total RO_x concentration consisted primarily of HO_2 (52%), isoprene peroxy radicals (20%), methyl peroxy

4   (CH_3O_2, 22%), and acetyl peroxy (CH_3CO_3, 5%), with daytime (08:00 – 20:00) contributions of 48%, 26%, 19%, and 5% for

5   HO_2, isoprene peroxy, CH_3O_2, and CH_3CO_3, respectively. The MCM 3.3.1 model predicted that HO_2 (53%), isoprene peroxy

6   (16%), methyl peroxy (23%), acetyl peroxy (5%) were the major contributors to the modeled diurnal average total RO_x

7   concentration, with daytime contributions of 50%, 22%, 21%, and 6% (Fig. 7). Similar results were obtained from the RACM2

8   models (Fig S1). As discussed above, the configuration of the IU-FAGE instrument used in this study converted approximately

9   83% of isoprene peroxy radicals to HO_2 upon addition of NO and minimally converts methyl peroxy radicals to HO_2 (<5%)

10   (Lew et al., 2018). Thus, the majority of the contributing species to the measured HO_2^* are HO_2 and isoprene peroxy radicals

11   which together account for approximately 70% of the total peroxy radical concentration predicted by these models.

12   Measurements of the total HO_2 + RO_2 radical concentrations using an Ethane – Nitric Oxide Chemical Amplifier (ECHAMP)

13   were found to be in good agreement with the HO_2^* measurements reported here and are summarized in Kundu et al. (2019).

14   **3.3 Total OH reactivity measurements and model comparison**

15   The measured total OH reactivity and that calculated from measured OH sinks using both the RACM and MCM

16   mechanisms are shown in Fig. 8, where the measured OH reactivity is averaged into 2 hour bins. As illustrated in this figure,

17   the calculated OH reactivity was in relatively good agreement with the measured OH reactivity on some days and nights,

18   specifically 15-16 July, with missing reactivity observed later in the campaign. Overall, the averaged measured OH reactivity

19   varied between the instrumental limit of detection of 1 s^{-1} to a maximum of approximately 31s^{-1} with an overall diurnal average

20   value of approximately 13 s^{-1}.

21   The campaign diurnal averaged measured OH reactivity is shown in Fig. 9 along with the calculated total OH

22   reactivity from the measured OH sinks. On average, the calculated reactivity is in good agreement with the measurements. As

23   expected for this deciduous forest environment, isoprene was the dominant contributor making up 37% of the diurnally

24   averaged total reactivity, followed by OVOCs (28%), inorganics (10%), alkanes and alkenes (5%), anthropogenic non-methane

25   hydrocarbons (NMHC) (1%), and monoterpenes (<1%) with missing reactivity accounting for the remaining 18% (Fig. S2).

26   During the daytime (08:00 and 20:00) the contributions are similar, with isoprene being the largest contributor at 47% followed

27   by OVOCs (24%), inorganics (8%), alkanes and alkenes (4%), anthropogenic NMHC (1%), and monoterpenes (<1%) with

28   missing reactivity accounting for the remaining 14%. During the nighttime, (20:00 to 08:00), OVOCs were the dominant

29   contributor to the modeled OH reactivity at 32% followed by isoprene (24%), inorganics (11%), alkanes and alkenes (6%),

30   anthropogenic NMHC (2%), and monoterpenes (<1%) with missing reactivity of 24% (Fig. S2).

31   The campaign diurnal average (Fig. 9) shows a correlation with temperature, with the maximum average OH

32   reactivity of approximately 20 s^{-1} occurring around 13:30. The calculated reactivity was consistent with the measured reactivity

33   for temperatures less than 294 K, while the observed reactivity is greater than that calculated from the measured sinks for

1   higher temperatures, although at temperatures above 302 K the measured reactivity appears to be less than calculated (Fig S3).

2   These results are similar to that reported by Hansen et al. (2014) and Di Carlo et al. (2004) in which the measured missing

3   reactivity appeared to increase with temperature.

4   Figure 9 also shows the campaign average OH reactivity including the reactivity of unmeasured oxidation products

5   predicted by the MCM 3.3.1 model. On average, including the contribution of unmeasured oxidation products can account for

6   the majority of the missing reactivity. While the model tends to overpredict the average measured reactivity in the afternoon

7   and evening, the model results agree to within the combined uncertainty of the model and the precision of the measurement

8   (Hansen et al., 2014). Similar results were obtained by the RACM2 models, although the predicted reactivity of unmeasured

9   oxidation products by the RACM2 models are approximately a factor of two smaller than that predicted by the MCM models

10   (Fig. S4). These results suggest that the models are generally able to reproduce the measured OH reactivity at this site, and

11   that the missing reactivity observed during IRRONIC may be due to unmeasured oxidation products, with isoprene nitrates

12   and isoprene epoxides within the RACM2 and MCM mechanisms being the primary contributors to the missing reactivity.

13   While the campaign averaged OH reactivity measurements appear to be in reasonable agreement with the calculated

14   reactivity based on measured compounds, there were several days that displayed large missing reactivity similar to that

15   observed by Hansen et al. (2014). The MCM 3.3.1 model results for a day with the largest missing reactivity (17 July) is shown

16   in Fig. 10, indicating that the modeled reactivity including unmeasured oxidation products cannot explain the observed

17   reactivity on this day. The reason for this discrepancy is unclear, but may indicate the presence of additional unmeasured

18   emissions or oxidation products not accounted for by the model.

19   **3.4 Radical budgets**

20   The analysis of the rates of radical initiation, propagation, and termination can provide insight to the importance of

21   individual radical sources and sinks. For the IRRONIC campaign, the OH radical budget is illustrated in Fig. 11, where OH

22   radical production reactions are represented in shades of blue and loss reactions are represented in shades of red. Daytime

23   production includes reactions with both initiation and propagation that produces OH radicals (positive rates), while daytime

24   OH loss reactions are represented by propagation and termination reactions that remove OH (negative rates). For simplicity

25   only the RACM2 and RACM2-LIM1 radical budgets are shown.

26   The maximum rates for the OH radical budget of approximately 2.8×10^7 cm^{-3} s^{-1} from the RACM2-LIM1 model

27   were higher than the maximum value of 2.2×10^7 cm^{-3} s^{-1} in RACM2. The addition of the LIM1 mechanism increases the OH

28   radical production rate mostly from photolysis of hydroxyperoxy aldehydes (HPALD) produced from the isomerization of

29   isoprene-based peroxy radicals and their subsequent chemistry (Peeters et al., 2014; Tan et al., 2017). In the RACM2-LIM1

30   model, the daytime OH radical production is dominated by the HO_2 + NO reaction from 10:00 to 14:00 (57%) and drops to

31   28% from 14:00 to 18:00. Ozone photolysis and the LIM1 mechanism contribute up to 24% and 31% of the total OH radical

32   production from 14:00 to 18:00, with ozonolysis (VOC+O_3) and photolysis of HONO, H_2O_2, methacrolein (MACR), and

33   organic peroxides (OP1, OP2) contributing to 13% and 4% of the total OH radical production in the afternoon (Fig. 11). A

1 majority of the OH radical loss is due to OH reactions with VOCs (66-72%) and OVOCs (22-19%) during the morning and

2 afternoon. As described above, the measured total OH reactivity was in reasonable agreement with the modeled OH reactivity;

3 therefore, it is likely that the total OH loss is well represented in the model.

4 The total radical (RO_x) budget from the RACM2 mechanisms of OH, HO_2, and RO_2 radicals is illustrated in Fig. 12.

5 Overall, total radical initiation in the RACM2-LIM1 mechanism was larger, with a maximum value of approximately 2.6 ×

6 10^7 cm^{-3} s^{-1} compared to RACM2 maximum value of approximately 1.7 × 10^7 cm^{-3} s^{-1}. The increase in total radical initiation

7 in the RACM2-LIM1 model is due to both the added radical initiation from the photolysis of HPALDs as well as increased

8 radical initiation from other aldehydes produced in the LIM1 mechanism. Overall, radical initiation from the photolysis of

9 HPALDs and the subsequent chemistry from the LIM1 mechanism contributed 8-11% of total radical initiation during the day,

10 while photolysis of formaldehyde and other aldehydes contributed to approximately 42% of total radical initiation, with ozone

11 photolysis contributing to 34-37% of radical initiation in the mornings and afternoon (Fig. 12). In contrast, ozone photolysis

12 contributes to approximately 50% of radical initiation in the RACM2 mechanism compared to formaldehyde and other

13 aldehydes contributing 31-34% (Fig. 12). Radical termination for both mechanisms is dominated by peroxy radical self-

14 reactions, such as the HO_2 + HO_2 reaction, as well as the reaction of HO_2 with isoprene-based peroxy radicals (ISOP) and

15 other peroxy radicals (RO_2). These reactions account for approximately 90-95% of radical termination due to the low levels

16 of NO_x used in the models, with reaction of OH +NO_2 and other NO_x radical reactions accounting for approximately 5-10%

17 of radical termination in these models (Fig. 12). As discussed above, it is possible that the NO concentration used to constrain

18 the model may be lower than the actual concentration. As a result, the modeled contribution of NO_x reactions to radical

19 termination may represent a lower limit to the actual contribution.

20 The partitioning of the total radical budget production for IRRONIC is similar to the modeled budget observed during

21 PROPHET 2008 and CABINEX 2009 (Griffith et al., 2013). The updated RACM model used during these campaigns predicted

22 that radical termination was dominated by HO_2 + RO_2 reactions (including the HO2 + ISOP reaction), contributing to

23 approximately 80% of total radical termination, similar to the 70-78% for the HO_2+ISOP and HO_2+RO_2 reactions predicted

24 here by the RACM2 model. The photolysis of ozone accounted for approximately 20-30% of total radical initiation during

25 these campaigns based on an updated version of the RACM model (Griffith et al., 2013) compared to approximately 50%

26 predicted by the RACM2 mechanism during IRRONIC due to higher concentrations observed during this campaign.

27 Ozonolysis reactions contributed to approximately 20-30% of total radical initiation during PROPHET and CABINEX

28 compared to 10-14% during IRRONIC. Photolysis of aldehydes, including HCHO, contributed to approximately 30% of the

29 total rate of radical initiation during IRRONIC compared to 23% and 5% during PROPHET 2008 and CABINEX 2009,

30 respectively, with the low contribution during CABINEX primarily due to the lower mixing ratios of HCHO observed during

31 this campaign (Griffith et al., 2013). In contrast, photolysis of HONO was a significant radical source during PROPHET and

32 CABINEX, contributing 14-17% of radical initiation compared to approximately 5% of total radical production during

33 IRRONIC due to the lower mixing ratios of HONO observed during IRRONIC. On average, mixing ratios of HONO during

34 IRRONIC were approximately 40 ppt at night decreasing to approximately 10 ppt during the day (Fig. S5) compared to daytime

Atmospheric
Chemistry
and Physics
Discussions

1 mixing ratios between 50 and 75 ppt during PROPHET and CABINEX (Griffith et al., 2013). The reason for the difference in

2 the measured HONO values between these two sites is unclear, but may be related to increased production from photolysis of

3 nitric acid on the forest canopy surfaces at the PROPHET site (Zhou et al., 2011).

4 **4 Summary**

5   Measurements of OH radical concentrations using the IU-FAGE instrument during the IRRONIC campaign revealed

6 a significant unknown interference that appeared to correlate with both temperature and ozone. The average measured OH

7 radical concentration after the interference was subtracted reached an average daytime maximum of approximately $4\text{-}5 \times 10^6$

8 cm^{-3}. This is in contrast to the measurements including the interference which reached an average daytime maximum of

9 approximately 9×10^6 cm^{-3}. Similar OH concentrations were observed at this site in 2017 during an informal intercomparison

10 between the IU-FAGE instrument and the University of Colorado Chemical Ionization Mass Spectrometry (CIMS) instrument

11 (Rosales et al., 2018; Reidy et al., 2018).

12   After subtracting the interference, the OH measurements were in better agreement with model simulations utilizing

13 the Regional Atmospheric Chemical Mechanism 2 (RACM2) with an updated Leuven Isoprene Mechanism (LIM1) as well as

14 the Master Chemical Mechanism versions 3.2 and 3.3.1. Both the RACM2-LIM1 and MCM 3.3.1 mechanisms add radical

15 recycling reactions for isoprene oxidation that increase the modeled OH and peroxy radical concentrations. The addition of

16 radical recycling by isoprene still resulted in model predictions of OH that were approximately a factor of two lower than the

17 measured concentrations. One possible explanation for the discrepancy is an underestimation of the mixing ratio of NO during

18 the campaign, as instrumental difficulties prevented measurements of NO except at the end of the campaign. Unconstraining

19 the mixing ratios of NO in the model while constraining NO_2 and O_3 to their measured values leads to an increase in the

20 modeled mixing ratios of NO resulting in an increase in the average modeled OH concentration by approximately a factor of

21 2-3, improving the agreement with the measured OH concentrations. These higher values of NO_x are comparable to that

22 observed at this site in 2017 when measured OH concentrations were similar to that observed here (Rosales et al., 2018; Reidy

23 et al., 2018). However, it is clear that if the measured interference was not taken into account, the apparent OH concentrations

24 would have been a factor of 5 greater than predicted by the model mechanisms, comparable to previous measurements under

25 low NO_x and high isoprene conditions (Rhorer et al., 2014). These results are similar to that reported by Mao et al. (2012) who

26 found good agreement between their OH measurements and model predictions when measured interferences are taken into

27 account. However, because of differences in instrument design (geometry, cell pressure, flow, etc.) these interference

28 measurements may not apply to other LIF-FAGE instruments. However, future OH measurements using the LIF-FAGE

29 technique should include methods to quantify potential instrumental artifacts.

30   Measurements of total OH reactivity were in reasonable agreement with that calculated from measured OH sinks,

31 with isoprene contributing approximately 37% and OVOCs 28% of the diurnally averaged measured reactivity, with 18% of

32 the measured reactivity missing. However, on average the missing reactivity fraction can be explained by unmeasured

1   oxidation products, specifically from isoprene nitrates and isoprene epoxides within the RACM2 and MCM mechanisms. This

2   indicates that these mechanisms are accurately representing the total OH loss at this site.

3   Measurements of HO_2 radicals by the IU-FAGE instrument using chemical conversion to OH by addition of NO has

4   been shown to be sensitive to alkene-based peroxy radicals (Lew et al., 2018). As a result, the measurements represent a sum

5   of HO_2 and a fraction of RO_2 radicals in the atmosphere (HO_2^*). During the IRRONIC campaign, the measured HO_2^*

6   concentration primarily reflected the sum of HO_2 and isoprene-based peroxy radicals, which contributed to approximately 70%

7   of the total modeled peroxy radicals. The average daytime ambient HO_2^* measurements reached maximum concentrations of

8   approximately 1×10^9 cm^{-3}. Both MCM models predicted HO_2^* concentrations that were in good agreement with the

9   measurements, while the RACM mechanisms resulting in predicted concentrations that were approximately 20-35% greater

10   than the measurements but within the combined uncertainty of both the model and the measurement. These results are also

11   consistent with an underestimation of the NO concentrations in the model, as increasing the modeled NO resulted in modeled

12   HO_2^* concentrations that were still in good agreement with the measurements. These results are in contrast to some previous

13   measurements in forest environments where model predictions were found to be significantly greater than measured HO_2^*

14   concentrations (Griffith et al., 2013), perhaps as a result of the lower mixing ratios of NO observed at these sites. Additional

15   measurements are needed in order to resolve this discrepancy, which may be related to a gap in our understanding of peroxy

16   radical chemistry under low NO conditions.

Data availability. Data are available upon request from the corresponding author (pstevens@indiana.edu).

Competing interests. The authors declare that they have no conflicts of interest.

Author contributions. PS, SD and EW designed the research project. ML, PR, BB, and PS were responsible for the LIF-FAGE OH, HO_2^*, OH reactivity, and HONO measurements. SK and EW were responsible for the supporting measurements of NO, NO_2, and O_3. SD, SS, TL, and NL were responsible for the measurements of VOCs and OVOCs. ML, PR, and PS conducted the analysis and photochemical modelling and wrote the paper with feedback from all co-authors. ML and PR contributed equally to the paper.

Atmospheric
Chemistry
and Physics
Discussions

Open Access

EGU

References

Ait-Helal, W., Borbon, A., Sauvage, S., de Gouw, J. A., Colomb, A., Gros, V., Freutel, F., Crippa, M., Afif, C., Baltensperger, U., Beekmann, M., Doussin, J.-F., Durand-Jolibois, R., Fronval, I., Grand, N., Leonardis, T., Lopez, M., Michoud, V., Miet, K., Perrier, S., Prévôt, A. S. H., Schneider, J., Siour, G., Zapf, P., and Locoge, N.: Volatile and intermediate volatility organic compounds in suburban Paris: variability, origin and importance for SOA formation, Atmos. Chem. Phys., 14, 10439–10464, 2014

Badol, C., Borbon, A., Locoge, N., Leonardis, T., and Galloo, J. C.: An automated monitoring system for VOC ozone precursors in ambient air: development, implementation and data analysis, Anal. Bioanal. Chem., 378, 7, 1815–1827, 2004.

Bottorff, B., Stevens, P. S., Lew, M., Rickly, P., and Dusanter, S. Measurements of Nitrous Acid (HONO) in an Indiana Forest by Laser Photofragmentation/Laser-Induced Flourescence (LP/LIF), Abstract A21B-0116 presented at 2015 Fall Meeting, AGU, San Francisco, CA, 14-18 Dec., 2015.

Bottorff, B., Lew, M., Mielke, L., Dusanter, S., and Stevens, P. S. Development of a new Laser Photo-fragmentation/Fluorescent Assay by Gas Expansion (LP/FAGE) technique for the measurement of tropospheric nitrous acid, Atmos. Meas. Tech., in preparation.

Carslaw, N., Creasey, D. J., Harrison, D., Heard, D. E., Hunter, M. C., Jacobs, P. J., Jenkin, M. E., Lee, J. D., Lewis, A. C., Pilling, M. J., Saunders, S. M., and Seakins, P. W.: OH and HO$_2$ Radical Chemistry in a Forested Region of North-Western Greece, Atmos. Environ., 35, 4725-4737, 2001.

Chen, S., Ren, X., Mao, J., Chen, Z., Brune, W. H., Lefer, B., Rappenglück, B., Flynn, J., Olson, J., and Crawford, J. H.: A Comparison of Chemical Mechanisms Based on Tramp-2006 Field Data, Atmos. Environ., 44, 4116-4125, 2010.

Creasey, D. J., Heard, D. E., and Lee, J. D.: Eastern Atlantic Spring Experiment 1997 (Ease97) 1. Measurements of OH and HO2 Concentrations at Mace Head, Ireland, J. Geophys. Res., 107, 10.1029/2001jd000892, 2002.

Czader, B. H., Li, X., and Rappenglueck, B.: Cmaq Modeling and Analysis of Radicals, Radical Precursors, and Chemical Transformations, J. Geophys. Res., 118, 11,376-311,387, 10.1002/jgrd.50807, 2013.

Davis, D. D., Rodgers, M. O., Fischer, S. D., and Asai, K.: An Experimental Assessment of the O$_3$/H$_2$O Interference Problem in the Detection of Natural Levels of OH Via Laser Induced Fluorescence, Geophys. Res. Lett., 8, 69-72, 10.1029/GL008i001p00069, 1981a.

Davis, D. D., Rodgers, M. O., Fischer, S. D., and Heaps, W. S.: A Theoretical Assessment of the O$_3$/H$_2$O Interference Problem in the Detection of Natural Levels of OH Via Laser Induced Fluorescence, Geophys. Res. Lett., 8, 73-76, 10.1029/GL008i001p00073, 1981b.

Detournay, A., Sauvage, S., Locoge, N., Gaudion, V., Leonardis, T., Fronval, I., Kaluzny, P., and Galloo, J.-C.: Development of a sampling method for the simultaneous monitoring of straightchain alkanes, straight-chain saturated carbonyl compounds and monoterpenes in remote areas, J. Environ. Monit., 13, 983–990, 2011.

Di Carlo, P., Brune, W. H., Martinez, M., Harder, H., Lesher, R., Ren, X., Thornberrry, T., Carroll, M. A., Young, V., Shepson, P. B., Riemer, D., Apel, E., and Campbell, C.: Missing OH Reactivity in a Forest: Evidence for Unknown Reactive Biogenic VOCs. Science, 304, 5671, 2004.

Dusanter, S., Vimal, D., and Stevens, P. S.: Technical Note: Measuring Tropospheric OH and HO_2 by Laser-Induced Fluorescence at Low Pressure. A Comparison of Calibration Techniques, Atmos. Chem. Phys., 8, 321-340, 2008.

Dusanter, S., Vimal, D., Stevens, P. S., Volkamer, R., and Molina, L. T.: Measurements of OH and HO_2 concentrations during the MCMA-2006 field campaign – Part 1: Deployment of the Indiana University laser-induced fluorescence instrument, Atmos. Chem. Phys., 9, 1665–1685, 2009a.

Dusanter, S., Vimal, D., Stevens, P. S., Volkamer, R., Molina, L. T., Baker, A., Meinardi, S., Blake, D., Sheehy, P., Merten, A., Zhang, R., Zheng, J., Fortner, E. C., Junkermann, W., Dubey, M., Rahn, T., Eichinger, B., Lewandowski, P., Prueger, J., and Holder, H.: Measurements of OH and HO_2 Concentrations During the MCMA-2006 Field Campaign – Part 2: Model Comparison and Radical Budget, Atmos. Chem. Phys., 9, 6655-6675, 2009b.

Dusanter S. and Stevens, P. S.: Recent Advances in the Chemistry of OH and HO_2 Radicals in the Atmosphere: Field and Laboratory Measurements, in Advances in Atmospheric Chemistry, Volume 1, John R. Barker, Allison L. Steiner, and Timothy J. Wallington, Editors, World Scientific Publishing Co. Pte. Ltd, New Jersey, pp. 493-579, 2017.

Emmerson, K. M., Carslaw, N., Carpenter, L. J., Heard, D. E., Lee, J. D., and Pilling, M. J.: Urban Atmospheric Chemistry During the Puma Campaign 1: Comparison of Modelled OH and HO_2 Concentrations with Measurements, J. Atmos. Chem., 52, 143-164, 2005.

Emmerson, K. M., Carslaw, N., Carslaw, D. C., Lee, J. D., McFiggans, G., Bloss, W. J., Gravestock, T., Heard, D. E., Hopkins, J., Ingham, T., Pilling, M. J., Smith, S. C., Jacob, M., and Monks, P. S.: Free Radical Modelling Studies During the UK Torch Campaign in Summer 2003, Atmos. Chem. Phys., 7, 167-181, 2007.

Fittschen, C., Al Ajami, M., Batut, S., Ferracci, V., Archer-Nicholls, S., Archibald, A. T., and Schoemaecker, C.: ROOOH: a missing piece of the puzzle for OH measurements in low-NO environments?, Atmos. Chem. Phys., 19, 349-362, 2019.

Fuchs, H., Bohn, B., Hofzumahaus, A., Holland, F., Lu, K. D., Nehr, S., Rohrer, F., and Wahner, A.: Detection of HO2 by Laser-Induced Fluorescence: Calibration and Interferences from RO2 Radicals, Atmos. Meas. Tech., 4, 1209-1225, 2011.

Fuchs, H., Tan, Z., Hofzumahaus, A., Broch, S., Dorn, H. P., Holland, F., Künstler, C., Gomm, S., Rohrer, F., Schrade, S., Tillmann, R., and Wahner, A.: Investigation of Potential Interferences in the Detection of Atmospheric RO_x Radicals by Laser-Induced Fluorescence under Dark Conditions, Atmos. Meas. Tech., 9, 1431-1447, 2016.

19

George, L. A., Hard, T. M., and O'Brien, R. J.: Measurement of Free Radicals OH and HO$_2$ in Los Angeles Smog, J. Geophys. Res., 104, 11643-11655, 10.1029/1998jd100113, 1999.

Goliff, W. S., Stockwell, W. R., and Lawson, C. V.: The Regional Atmospheric Chemistry Mechanism, Version 2, Atmos. Environ., 68, 174-185, 2013.

Griffith, S. M., Hansen, R. F., Dusanter, S., Stevens, P. S., Alaghmand, M., Bertman, S. B., Car-roll, M. A., Erickson, M., Galloway, M., Grossberg, N., Hottle, J., Hou, J., Jobson, B. T., Kammrath, A., Keutsch, F. N., Lefer, B. L., Mielke, L. H., O'Brien, A., Shepson, P. B., Thurlow, M., Wallace, W., Zhang, N., and Zhou, X. L.: OH and HO$_2$ Radical Chemistry During PROPHET 2008 and CABINEX 2009 - Part 1: Measurements and Model Comparison, Atmos. Chem. Phys., 13, 5403-5423, 2013.

Griffith, S. M., Hansen, R. F., Dusanter, S., Michoud, V., Gilman, J. B., Kuster, W. C., Veres, P. R., Graus, M., de Gouw, J. A., Roberts, J., Young, C., Washenfelder, R., Brown, S. S., Thalman, R., Waxman, E., Volkamer, R., Tsai, C., Stutz, J., Flynn, J. H., Grossberg, N., Lefer, B., Alvarez, S. L., Rappenglueck, B., Mielke, L. H., Osthoff, H. D., and Stevens, P. S.: Measurements of Hydroxyl and Hydroperoxy Radicals During CalNex-LA: Model Comparisons and Radical Budgets, J. Geophys. Res., 121, 4211-4232, 10.1002/2015JD024358, 2016.

Hansen, R. F., Griffith, S. M., Dusanter, S., Rickly, P. S., Stevens, P. S., Bertman, S. B., Carroll, M. A., Erickson, M. H., Flynn, J. H., Grossberg, N., Jobson, B. T., Lefer, B. L., and Wallace, H. W.: Measurements of total hydroxyl radical reactivity during CABINEX 2009 – Part 1: field measurements. Atmos. Chem. Phys., 14, 2923-2937, 2014.

Heard, D. E., and Pilling, M. J.: Measurement of OH and HO$_2$ in the Troposphere, Chem. Rev., 103, 5163-5198, 2003.

Hens, K., Novelli, A., Martinez, M., Auld, J., Axinte, R., Bohn, B., Fischer, H., Keronen, P., Kubistin, D., Nölscher, A. C., Oswald, R., Paasonen, P., Petäjä, T., Regelin, E., Sander, R., Sinha, V., Sipilä, M., Taraborrelli, D., Tatum Ernest, C., Williams, J., Lelieveld, J., and Harder, H.: Observation and Modelling of HO$_x$ Radicals in a Boreal Forest, Atmos. Chem. Phys., 14, 8723-8747, 2014.

Hofzumahaus, A., Rohrer, F., Lu, K., Bohn, B., Brauers, T., Chang, C.-C., Fuchs, H., Holland, F., Kita, K., Kondo, Y., Li, X., Lou, S., Shao, M., Zeng, L., Wahner, A., and Zhang, Y.: Amplified Trace Gas Removal in the Troposphere, Science, 324, 1702-1704, 2009.

Holland, F., Hofzumahaus, A., Schäfer, J., Kraus, A., and Pätz, H.-W.: Measurements of OH and HO$_2$ Radical Concentrations and Photolysis Frequencies During Berlioz, J. Geophys. Res., 108, 8246, doi:8210.1029/2001JD001393, 2003.

Jenkin, M. E., Saunders, S. M., Pilling, M. J. The Tropospheric Degredation of Volatile Organic Compounds: A Protocol for Mechanism Development, Atmos. Environ., 31, 81, 1997.

Jenkin, M. E., Young, J. C., and Rickard, A. R.: The MCM v3.3.1 degradation scheme for isoprene, Atmos. Chem. Phys., 15, 11433-11459, 2015.

Kanaya, Y., Sadanaga, Y., Hirokawa, J., Kajii, Y., and Akimoto, H.: Development of a Ground-Based LIF Instrument for Measuring HO$_x$ Radicals: Instrumentation and Calibrations, J. Atmos. Chem., 38, 73-110, 2001.

Atmospheric
Chemistry
and Physics
Discussions
Open Access
EGU

Kanaya, Y., Cao, R., Akimoto, H., Fukuda, M., Komazaki, Y., Yokouchi, Y., Koike, M., Tanimoto, H., Takegawa, N., and Kondo, Y.: Urban Photochemistry in Central Tokyo: 1. Observed and Modeled OH and HO_2 Radical Concentrations During the Winter and Summer of 2004, J. Geophys. Res., 112, 10.1029/2007jd008670, 2007a.

Kanaya, Y., Cao, R., Kato, S., Miyakawa, Y., Kajii, Y., Tanimoto, H., Yokouchi, Y., Mochida, M., Kawamura, K., and Akimoto, H.: Chemistry of OH and HO_2 Radicals Observed at Rishiri Island, Japan, in September 2003: Missing Daytime Sink of HO_2 and Positive Nighttime Correlations with Monoterpenes, J. Geophys. Res., 112, doi:10.1029/2006JD007987, 2007b.

Kanaya, Y., Hofzumahaus, A., Dorn, H. P., Brauers, T., Fuchs, H., Holland, F., Rohrer, F., Bohn, B., Tillmann, R., Wegener, R., Wahner, A., Kajii, Y., Miyamoto, K., Nishida, S., Watanabe, K., Yoshino, A., Kubistin, D., Martinez, M., Rudolf, M., Harder, H., Berresheim, H., Elste, T., Plass-Dülmer, C., Stange, G., Kleffmann, J., Elshorbany, Y., and Schurath, U.: Comparisons of Observed and Modeled OH and HO_2 Concentrations During the Ambient Measurement Period of the HOxComp Field Campaign, Atmos. Chem. Phys., 12, 2567-2585, 2012.

Kim, S., Wolfe, G. M., Mauldin, L., Cantrell, C., Guenther, A., Karl, T., Turnipseed, A., Green-berg, J., Hall, S. R., Ullmann, K., Apel, E., Hornbrook, R., Kajii, Y., Nakashima, Y., Keutsch, F. N., DiGangi, J. P., Henry, S. B., Kaser, L., Schnitzhofer, R., Graus, M., Han-sel, A., Zheng, W., and Flocke, F. F.: Evaluation of HO_x Sources and Cycling Using Measurement-Constrained Model Calculations in a 2-Methyl-3-Butene-2-ol (MBO) and Monoterpene (MT) Dominated Ecosystem, Atmos. Chem. Phys., 13, 2031-2044, 2013.

Konrad, S., Schmitz, T., Buers, H. J., Houben, N., Mannschreck, K., Mihelcic, D., Müsgen, P., Pätz, H. W., Holland, F., Hofzumahaus, A., Schäfer, H. J., Schröder, S., Volz-Thomas, A., Bächmann, K., Schlomski, S., Moortgat, G., and Großmann, D.: Hydrocarbon Measurements at Pabstthum During the Berlioz Campaign and Modeling of Free Radicals, J. Geophys. Res., 108, 8251, 10.1029/2001jd000866, 2003.

Kubistin, D., Harder, H., Martinez, M., Rudolf, M., Sander, R., Bozem, H., Eerdekens, G., Fischer, H., Gurk, C., Klüpfel, T., Königstedt, R., Parchatka, U., Schiller, C. L., Stickler, A., Taraborrelli, D., Williams, J., and Lelieveld, J.: Hydroxyl Radicals in the Tropical Troposphere over the Suriname Rainforest: Comparison of Measurements with the Box Model Mecca, Atmos. Chem. Phys., 10, 9705-9728, 2010.

Kundu, S., Deming, B. L., Lew, M. M., Bottorff, B. P., Rickly, P., Stevens, P. S., Dusanter, S., Sklaveniti, S., Leonardis, T., Locoge, N., and Wood, E. C.: Peroxy Radical Measurements by ethane – nitric oxide chemical amplification and laser-induced fluorescence during the IRRONIC field campaign in a forest in Indiana, Atmos. Chem. Phys. 19, 9563-9579, 2019.

Lelieveld, J., Butler, T. M., Crowley, J. N., Dillon, T. J., Fischer, H., Ganzeveld, L., Harder, H., Lawrence, M. G., Martinez, M., Taraborrelli, D., and Williams, J.: Atmospheric Oxidation Capacity Sustained by a Tropical Forest, Nature, 452, 737-740, 2008.

Levy, H.: Photochemistry of the Lower Troposphere, Planetary and Space Science, 20, 919-935, 1972.

Lew, M. M., Dusanter, S., and Stevens, P. S.: Measurement of Interferences Associated with the Detection of the Hydroperoxy Radical in the Atmosphere Using Laser-Induced Fluorescence, Atmos. Meas. Tech., 11, 95–109, 2018.

Lu, K. D., Hofzumahaus, A., Holland, F., Bohn, B., Brauers, T., Fuchs, H., Hu, M., Häseler, R., Kita, K., Kondo, Y., Li, X., Lou, S. R., Oebel, A., Shao, M., Zeng, L. M., Wahner, A., Zhu, T., Zhang, Y. H., and Rohrer, F.: Missing OH Source in a Suburban Environment near Beijing: Observed and Modelled OH and HO_2 Concentrations in Summer 2006, Atmos. Chem. Phys., 13, 2013.

Mao, J., Ren, X., Zhang, L., Van Duin, D. M., Cohen, R. C., Park, J. H., Goldstein, A. H., Pau-lot, F., Beaver, M. R., Crounse, J. D., Wennberg, P. O., DiGangi, J. P., Henry, S. B., Keutsch, F. N., Park, C., Schade, G. W., Wolfe, G. M., Thornton, J. A., and Brune, W. H.: Insights into Hydroxyl Measurements and Atmospheric Oxidation in a California Forest, Atmos. Chem. Phys., 12, 8009-8020, 2012.

Martinez, M., Harder, H., Kovacs, T. A., Simpas, J. B., Bassis, J., Lesher, R., Brune, W. H., Frost, G. J., Williams, E. J., Stroud, C. A., Jobson, B. T., Roberts, J. M., Hall, S. R., Shetter, R. E., Wert, B., Fried, A., Alicke, B., Stutz, J., Young, V. L., White, A. B., and Zamora, R. J.: OH and HO_2 Concentrations, Sources, and Loss Rates During the Southern Oxidants Study in Nashville, Tennessee, Summer 1999, J. Geophys. Res., 108, 10.1029/2003jd003551, 2003.

Michoud, V., Kukui, A., Camredon, M., Colomb, A., Borbon, A., Miet, K., Aumont, B., Beekmann, M., Durand-Jolibois, R., Perrier, S., Zapf, P., Siour, G., Ait-Helal, W., Locoge, N., Sauvage, S., Afif, C., Gros, V., Furger, M., Ancellet, G., and Doussin, J. F.: Radical Budget Analysis in a Suburban European Site During the Megapoli Summer Field Campaign, Atmos. Chem. Phys., 12, 11951-11974, 2012.

Nölscher, A. C., Yañez-Serrano, A. M., Wolff, S., de Araujo, A. C., Lavrič, J. V., Kesselmeier, J., and Williams, J.: Unexpected seasonality in quantity and composition of Amazon rainforest air reactivity, Nature Communications, https://doi.org/10.1038/ncomms10383, 2016.

Novelli, A., Hens, K., Tatum Ernest, C., Kubistin, D., Regelin, E., Elste, T., Plass-Dülmer, C., Martinez, M., Lelieveld, J., and Harder, H.: Characterisation of an inlet pre-injector laser-induced fluorescence instrument for the measurement of atmospheric hydroxyl radicals, Atmos. Meas. Tech., 7, 3413-3430, 2014.

Novelli, A., Hens, K., Tatum Ernest, C., Martinez, M., Nölscher, A. C., Sinha, V., Paasonen, P., Petäjä, T., Sipilä, M., Elste, T., Plass-Dülmer, C., Phillips, G. J., Kubistin, D., Williams, J., Vereecken, L., Lelieveld, J., and Harder, H.: Estimating the Atmospheric Concentration of Criegee Intermediates and Their Possible Interference in a FAGE-LIF Instrument, Atmos. Chem. Phys., 17, 7807-7826, 2017.

Peeters, J., Nguyen, T. L., and Vereecken, L.: HO_x Radical Regeneration in the Oxidation of Isoprene, Phys. Chem. Chem. Phys., 11, 5935, 2009.

Peeters, J., Müller, J.-F., Stavrakou, T., and Nguyen, V. S.: Hydroxyl Radical Recycling in Isoprene Oxidation Driven by Hydrogen Bonding and Hydrogen Tunneling: The Upgraded LIM1 Mechanism, J. Phys. Chem. A, 118, 8625-8643, 2014.

Reidy, E., Rosales, C., Bottorff, B., Stevens, P. S., Cantrell, C. A., Mauldin, L. Anderson, D. C., and Wood, E. C. D. An Informal Intercomparison of Ambient OH, HO$_2$, and RO$_2$ Measurements in an Indiana Forest Part 2: Comparison with Model Predictions, Abstract A43M-3281 presented at 2018 Fall Meeting, AGU, Washington, D.C., 10-14 Dec., 2018.

Ren, X., Harder, H., Martinez, M., Lesher, R. L., Oliger, A., Simpas, J. B., Brune, W. H., Schwab, J. J., Demerjian, K. L., He, Y., Zhou, X., and Gao, H.: OH and HO$_2$ Chemistry in the Urban Atmosphere of New York City, Atmospheric Environment, 37, 3639-3651, 2003.

Ren, X., Brune, W., Cantrell, C., Edwards, G., Shirley, T., Metcalf, A., and Lesher, R.: Hydroxyl and Peroxy Radical Chemistry in a Rural Area of Central Pennsylvania: Observations and Model Comparisons, J. Atmos. Chem., 52, 231-257, 2005.

Ren, X., Brune, W. H., Oliger, A., Metcalf, A. R., Simpas, J. B., Shirley, T., Schwab, J. J., Bai, C., Roychowdhury, U., Li, Y., Cai, C., Demerjian, K. L., He, Y., Zhou, X., Gao, H., and Hou, J.: OH, HO$_2$, and OH Reactivity During the PMTACS-NY Whiteface Mountain 2002 Campaign: Observations and Model Comparison, J. Geophys. Res., 111, doi:10.1029/2005JD006126, 2006.

Ren, X., van Duin, D., Cazorla, M., Chen, S., Mao, J., Zhang, L., Brune, W. H., Flynn, J. H., Grossberg, N., Lefer, B. L., Rappenglück, B., Wong, K. W., Tsai, C., Stutz, J., Dibb, J. E., Thomas Jobson, B., Luke, W. T., and Kelley, P.: Atmospheric oxidation chemistry and ozone production: Results from SHARP 2009 in Houston, Texas, J. Geophys. Res., 118, 5770–5780, 2013.

Rickly, P., and Stevens, P. S.: Measurements of the OH Radical Yield from the Ozonolysis of Biogenic Alkenes: A Potential Interference with Laser-Induced Fluorescence Measurements of Ambient OH, Atmos. Meas. Tech. 11,1-16, 2018.

Rohrer, F., Lu, K., Hofzumahaus, A., Bohn, B., Brauers, T., Chang, C.-C., Fuchs, H., Haseler, R., Holland, F., Hu, M., Kita, K., Kondo, Y., Li, X., Lou, S., Oebel, A., Shao, M., Zeng, L., Zhu, T., Zhang, Y., and Wahner, A.: Maximum Efficiency in the Hydroxyl-Radical-Based Self-Cleansing of the Troposphere, Nature Geosci, 7, 559-563, 2014.

Rosales, C., Reidy, E., Bottorff, B., Stevens, P. S., Cantrell, C. A., Mauldin, L. Anderson, D. C., and Wood, E. C. D., An Informal Intercomparison of Ambient Measurements of OH, HO$_2$, and RO$_2$ Radicals in an Indiana Forest, Part 1: Comparison of Instrumental Measurements, Abstract A43M-3280 presented at 2018 Fall Meeting, AGU, Washington, D.C., 10-14 Dec., 2018.

Roukos, J., Plaisance, H., Leonardis, T., Bates, M., and Locoge, N.: Development and validation of an automated monitoring system for oxygenated volatile organic compounds and nitrile compounds in ambient air, J. Chromatr. A, 1216, 8642–8651, 2009.

Saunders, S. M., Jenkin, M. E., Derwent, R. G., and Pilling, M. J.: Protocol for the development of the Master Chemical Mechanism, MCM v3 (Part A): Tropospheric degradation of non-aromatic volatile organic compounds, Atmos. Chem. Phys., 3, 161-180, 2003.

Sheehy, P. M., Volkamer, R., Molina, L. T., and Molina, M. J.: Oxidative Capacity of the Mexico City Atmosphere – Part 2: A RO$_x$ Radical Cycling Perspective, Atmos. Chem. Phys., 10, 6993-7008, 2010.

Shetter, R. E., and M. Muller, Photolysis frequency measurements using actinic flux spectroradiometry during the PEM-Tropics mission: Instrumentation description and some results, J. Geophys. Res., 104, 5647–5661, doi:10.1029/98JD01381, 1999.

Shirley, T. R., Brune, W. H., Ren, X., Mao, J., Lesher, R., Cardenas, B., Volkamer, R., Molina, L. T., Molina, M. J., Lamb, B., Velasco, E., Jobson, T., and Alexander, M.: Atmospheric Oxidation in the Mexico City Metropolitan Area (MCMA) During April 2003, Atmos. Chem. Phys., 6, 2753-2765, 2006.

Sklaveniti, S., Locoge, N., Stevens, P. S., Wood, E., Kundu, S., and Dusanter, S.: Development of an instrument for direct ozone production rate measurements: measurement reliability and current limitations, Atmos. Meas. Tech., 11, 741-761, 2018.

Stevens, P. S., Mather, J. H., and Brune, W. H.: Measurement of Tropospheric OH and HO_2 by Laser-Induced Fluorescence at Low Pressure, J. Geophys. Res., 99, 3543-3557, 10.1029/93jd03342, 1994.

Tan, D., Faloona, I., Simpas, J. B., Brune, W., Shepson, P. B., Couch, T. L., Sumner, A. L., Carroll, M. A., Thornberry, T., Apel, E., Riemer, D., and Stockwell, W.: HOx Budgets in a Deciduous Forest: Results from the PROPHET Summer 1998 Campaign, J. Geophys. Res., 106, 24407-24427, 10.1029/2001jd900016, 2001.

Tan, Z., Fuchs, H., Lu, K., Hofzumahaus, A., Bohn, B., Broch, S., Dong, H., Gomm, S., Häseler, R., He, L., Holland, F., Li, X., Liu, Y., Lu, S., Rohrer, F., Shao, M., Wang, B., Wang, M., Wu, Y., Zeng, L., Zhang, Y., and Wahner, A.: Radical Chemistry at a Rural Site (Wangdu) in the North China Plain: Observation and Model Calculations of OH, HO_2 and RO_2 Radicals, Atmos. Chem. Phys., 17, 663-690, 2017.

Whalley, L. K., Edwards, P. M., Furneaux, K. L., Goddard, A., Ingham, T., Evans, M. J., Stone, D., Hopkins, J. R., Jones, C. E., Karunaharan, A., Lee, J. D., Lewis, A. C., Monks, P. S., Moller, S. J., and Heard, D. E.: Quantifying the Magnitude of a Missing Hydroxyl Radical Source in a Tropical Rainforest, Atmos. Chem. Phys., 11, 7223-7233, 2011.

Whalley, L. K., Blitz, M. A., Desservettaz, M., Seakins, P. W., and Heard, D. E.: Reporting the Sensitivity of Laser-Induced Fluorescence Instruments Used for HO_2 Detection to an Interference from RO_2 Radicals and Introducing a Novel Approach That Enables HO_2 and Certain RO_2 Types to Be Selectively Measured, Atmos. Meas. Tech., 6, 3425-3440, 2013.

Wolfe, G. M., Marvin, M. R., Roberts, S. J., Travis, K. R., and Liao, J.: The Framework for 0-D Atmospheric Modeling (F0AM) V3.1, Geosci. Model Dev., 9, 3309-3319, 2016.

Zannoni, N., Gros, V., Lanza, M., Sarda, R., Bonsang, B., Kalogridis, C., Preunkert, S., Legrand, M., Jambert, C., Boissard, C., and Lathiere, J.: OH reactivity and concentrations of biogenic volatile organic compounds in a Mediterranean forest of downy oak trees, Atmos. Chem. Phys., 16, 1619-1636, 2016.

Zhou, X., N. Zhang, M. TerAvest, D. Tang, J. Hou, S. Bertman, M. Alaghmand, P. B. Shepson, M. A. Carroll, S. Griffith, S. Dusanter and P. S. Stevens: Nitric acid photolysis on forest canopy surface as a source for tropospheric nitrous acid. Nature Geosci., 4, 440-443, 2011.

Atmospheric
Chemistry
and Physics
Discussions

Table 1: Measurements conducted during the IRRONIC field campaign.

Measurement	Instrument	Technique	LOD	Reference
OH	LIF-FAGE	Laser-induced fluorescence – fluorescence assay by gas expansion	8×10^5 cm^{-3} / 30 min	Dusanter et al., 2009a;
HO$_2$*			7×10^7 cm^{-3} / 20 s	Lew et al., 2018
NO	Thermo 42i-TL	Chemiluminescence	50 ppt / 2 min	
NO$_2$	Aerodyne CAPS	Cavity attenuated phase shift spectroscopy	40 ppt / 10 s	
Ozone	2B Technologies Model 202	UV absorbance	3 ppb / 10 s	
OH reactivity	LIF-TOHLM	Total OH Loss Measurement	1 s^{-1} (10 min)	Hansen et al., 2013
HONO	LP LIF-FAGE	Laser-photofragmentation laser-induced fluorescence	20 ppt (30 min)	Bottorff et al., in prep
NMHCs	Online GC/FID	Gas chromatography with flame ionization detection	10-100 ppt (1.5 hr)	Badol et al., 2004
OVOCs	Online GC/FID-MS	Gas chromatography with mass spectrometer and FID	5-100 ppt (1.5 hr)	Roukos et al. (2009)
	Off-line Sorbent GC-MS	Sorbent cartridges analyzed by GC-MS		Detournay et al. (2011); Ait-Helal et al. (2014)
	Off-line DNPH HPLC-UV	Dinitrophenylhydrazine cartridges analyzed by high-performance liquid chromatography with UV detection		
J(NO$_2$)		Spectral Radiometry	0.3×10^{-4} s^{-1}	Shetter and Muller (1999)
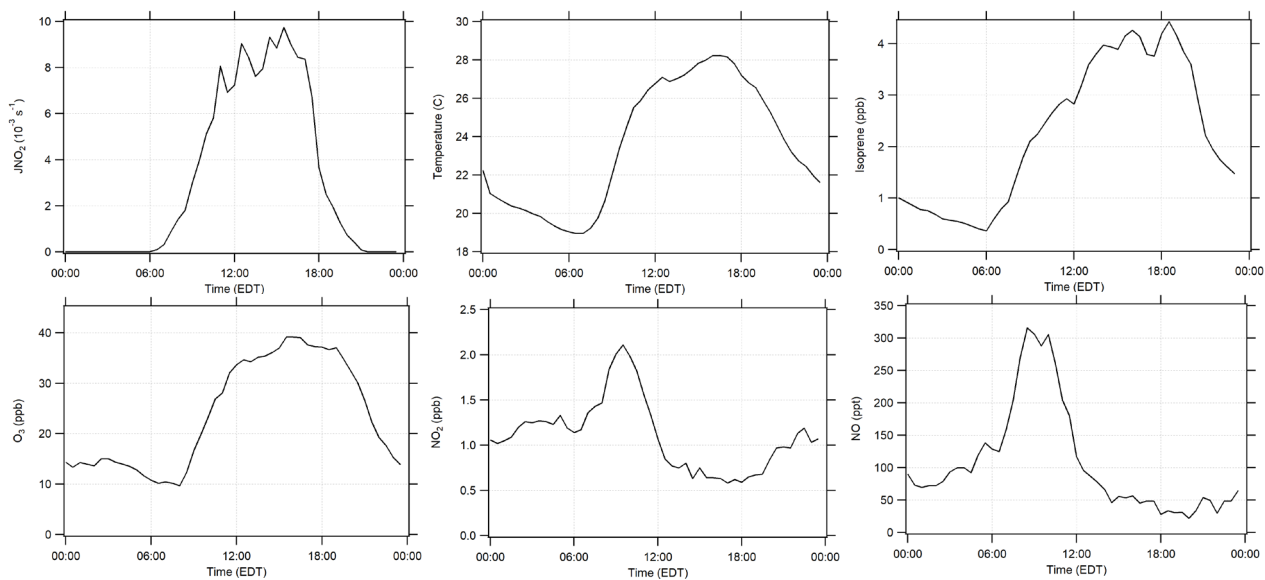
Figure 1. Diurnal campaign average profiles of J(NO$_2$), temperature, isoprene, O$_3$, NO$_2$, and NO.
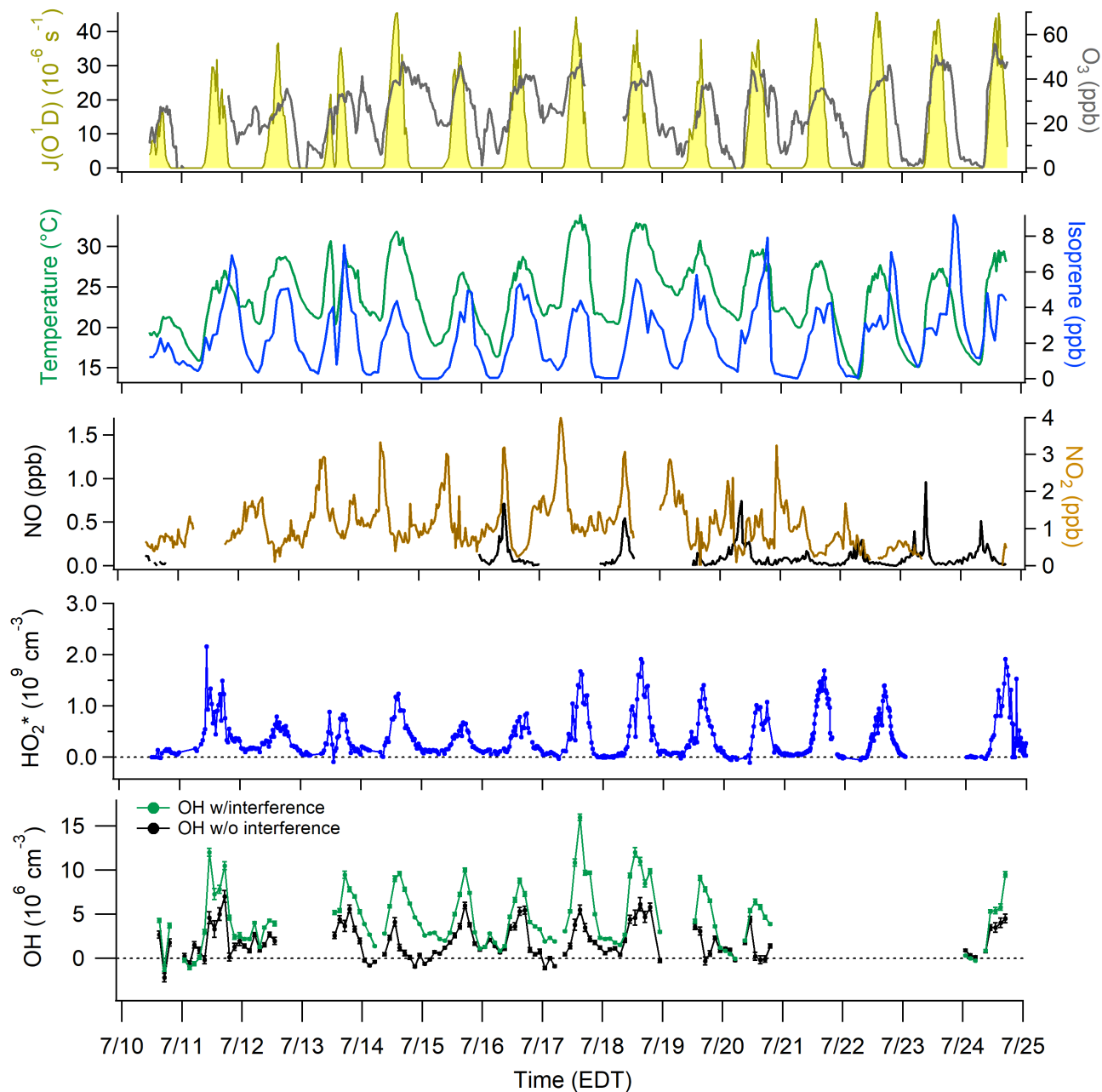
Figure 2. Time series of OH and HO₂* from July 10 to July 25 with model calculated J(O¹D) scaled to the measured J(NO₂), and measured ozone, temperature, isoprene, and NOₓ. OH measurements with interference (± 1σ) represented by the green line and measurements without interference (± 1σ) represented by the black line. For clarity, OH data shown are 2 hour averages. HO₂* data are 30 s averages every 30 minutes.
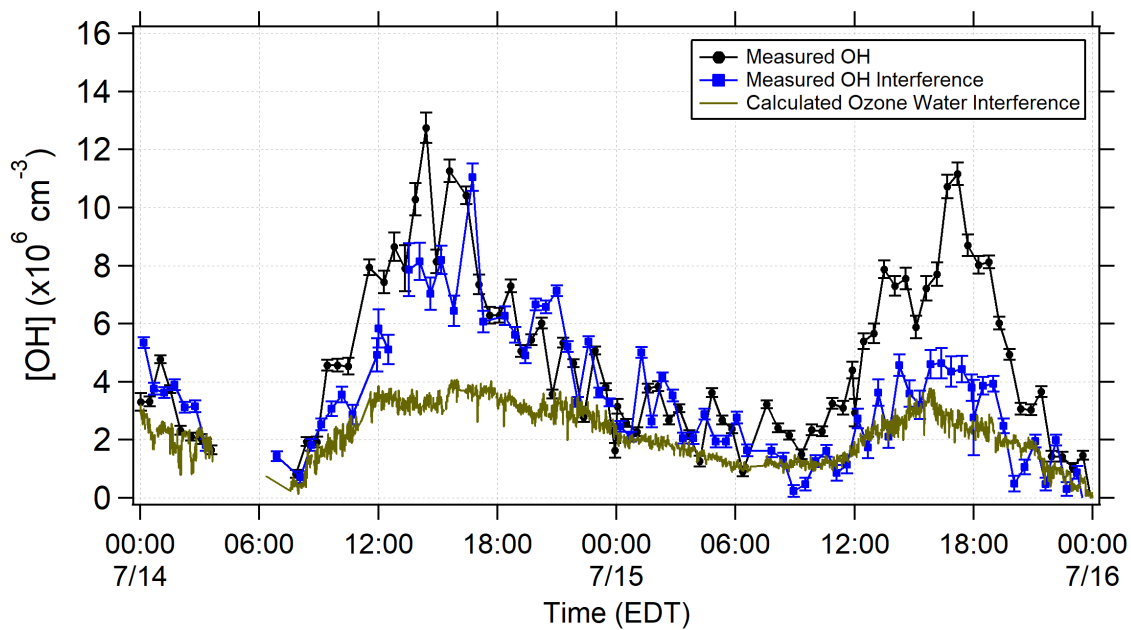
Figure 3. Averaged measured total OH signal using spectral modulation (black), and the measured interference using chemical modulation (blue) during July 14 and July 15. The calculated laser-generated interference from ozone photolysis for these days (reactions 1 and 2, green points) is also shown.
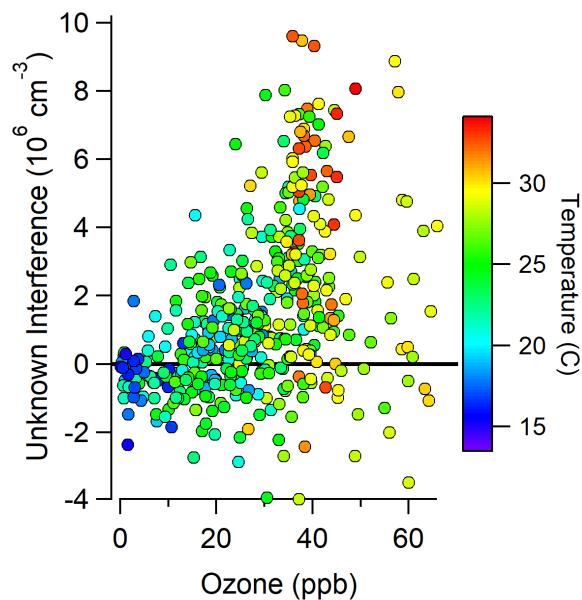
Figure 4. Measurements of the unknown interference as a function of ozone and temperature during the campaign.
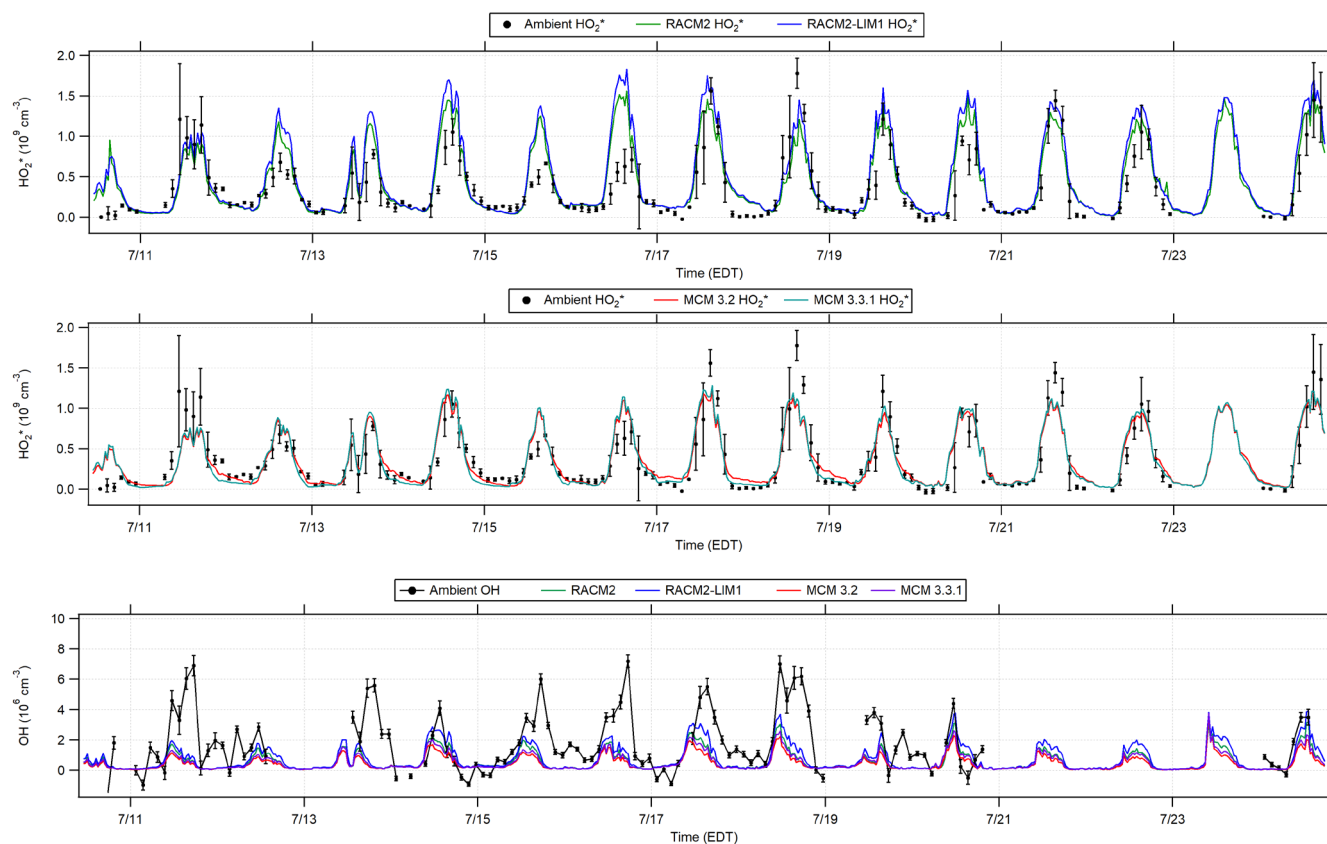
Figure 5. Average measurements of OH (bottom) and HO$_2$* from July 10 to July 25 during the IRRONIC campaign in comparison to modeled results for RACM2 and RACM2-LIM1 models (top) and the MCM 3.2 and MCM 3.3.1 models (middle). The error bars represent the precision of the measurements (1σ).
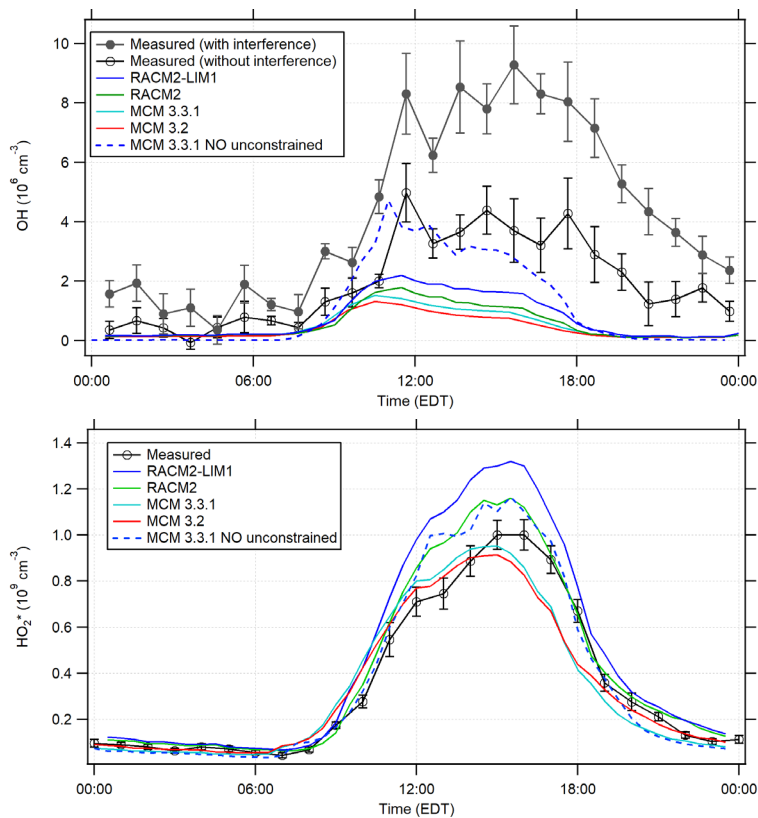
Figure 6. Diurnal profiles of OH (top) and HO$_2$* (bottom) with the RACM2, RACM2-LIM1, MCM 3.2, and MCM 3.3.1 model results. The open circles represent the 1 hour mean ± 1σ standard error of OH and HO$_2$* measurements. The filled circles represent the 1 hour mean ± 1σ standard error of the OH measurements with the interference. The dashed line represent the MCM 3.3.1 model results with NO concentrations unconstrained (see text).
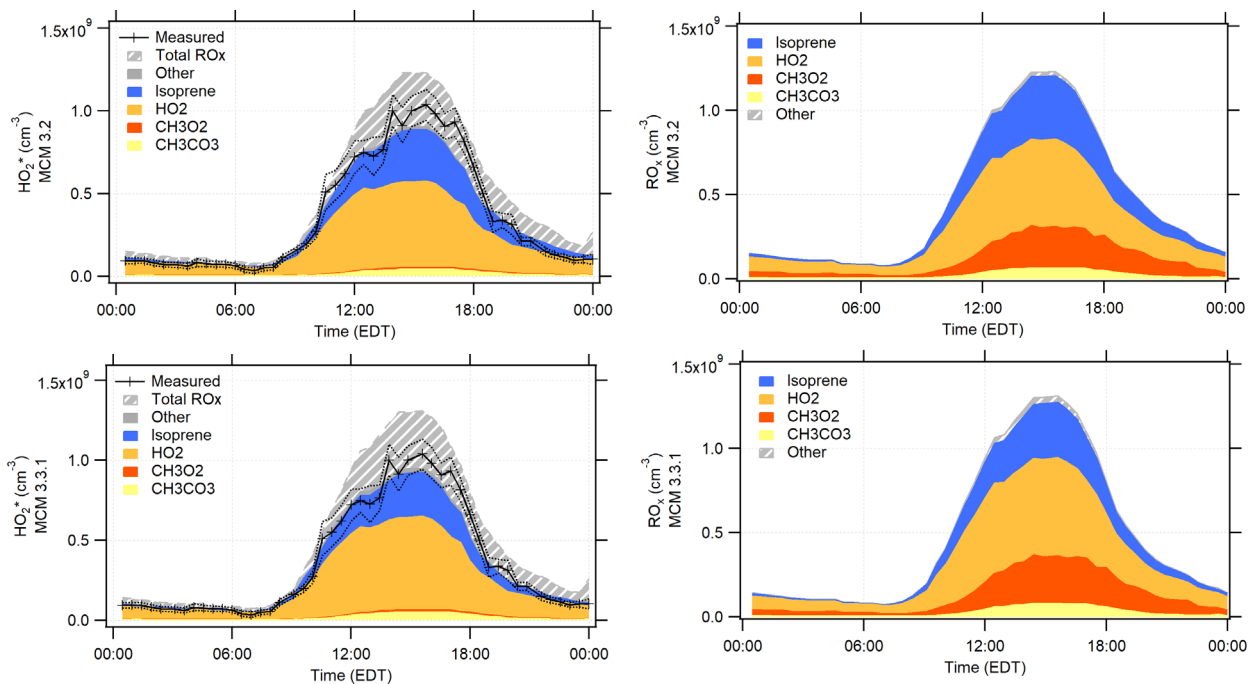
Figure 7. The MCM 3.2, and MCM 3.3.1 diurnal average modeled peroxy radical concentration and composition. Left panels show the modeled contribution to the measured HO$_2$* concentrations. The measured 30-min mean HO$_2$* concentrations are shown by the black line with ± 1σ standard error shown by the dotted lines. Right panels show the total RO$_x$ (RO$_2$ +HO$_2$) composition predicted by each model.
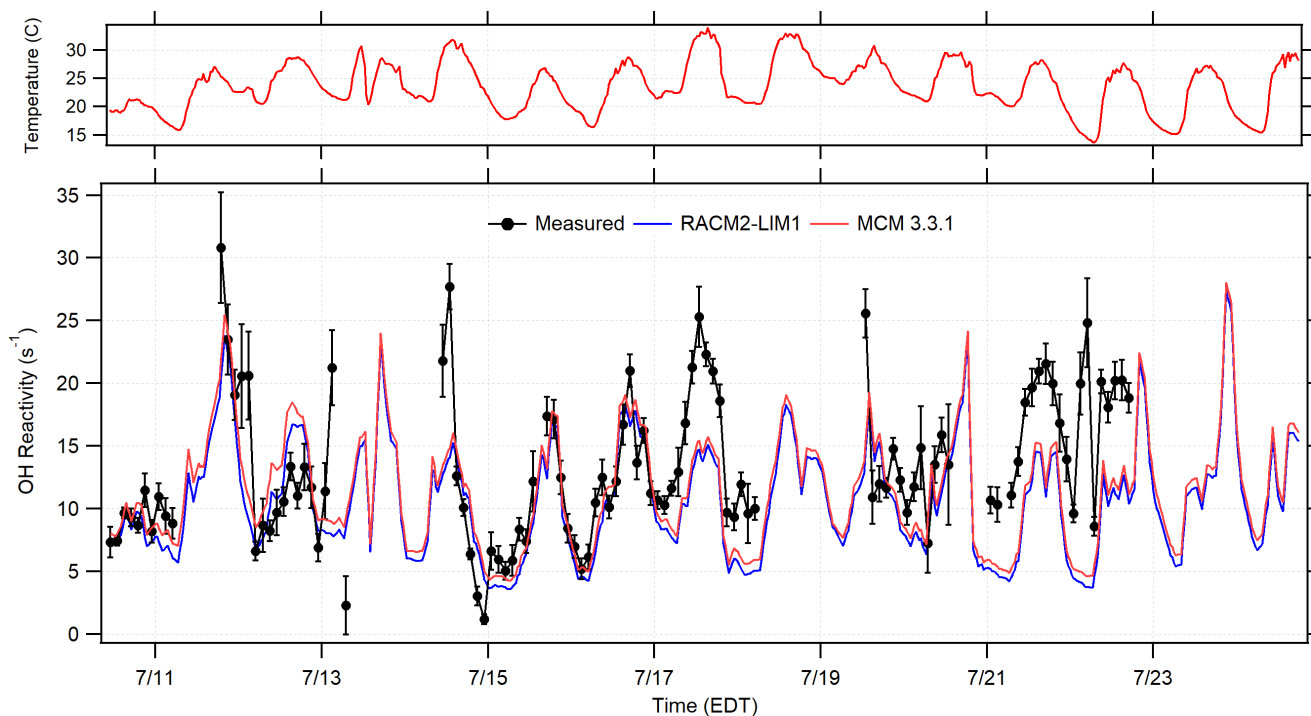
Figure 8. Time series of the 2 hour averaged OH reactivity measurements (black circles) in comparison to the RACM2-LIM1 and MCM 3.3.1 calculated OH reactivity based on measured OH sinks along with ambient temperature (top). Error bars represent the standard error of the average measurement.
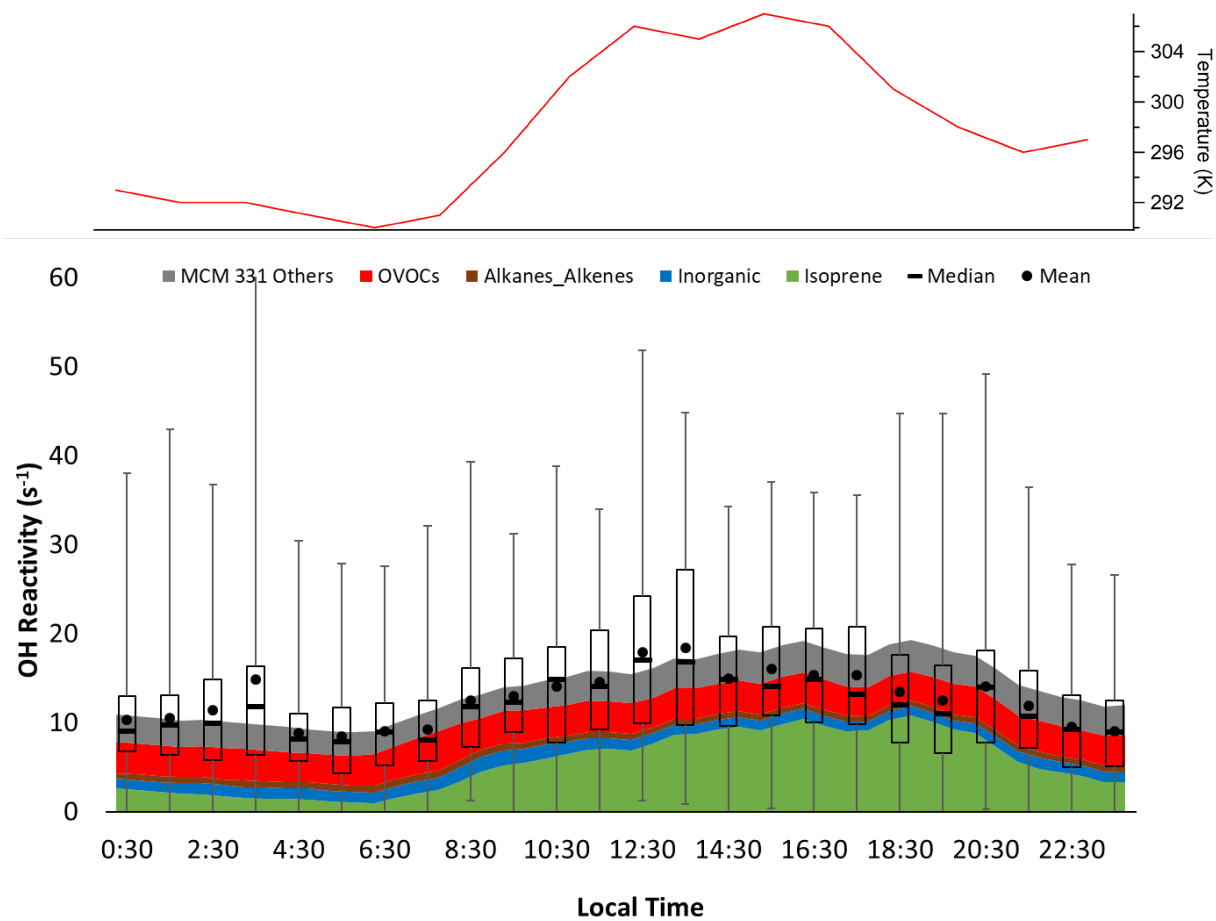
Figure 9. Diurnal temperature (top) and box and whiskers plot of observed total OH reactivity showing the mean and median values for each hour, with the mean calculated values from the measured OH sinks as well as the unmeasured oxidation products from the MCM 3.3.1 model results (Others). Error bars show the range of individual 5-min measurements and bars show Q1 and Q3 for the measured OH reactivity.
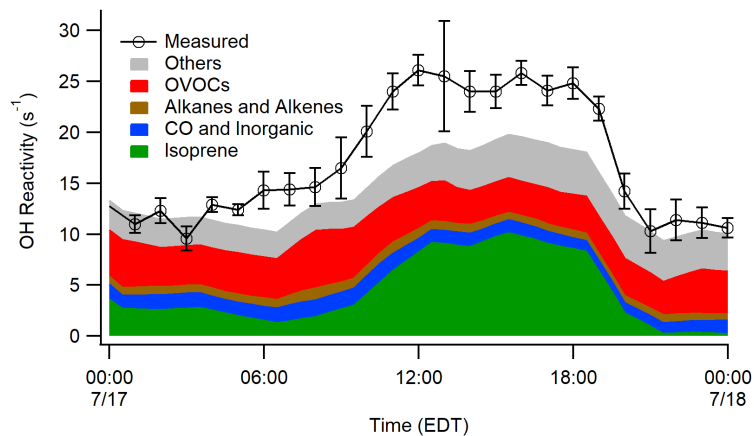
Figure 10. Median diurnally averaged OH reactivity from July 17 in comparison to modeled reactivity from the MCM 3.3.1 mechanism.
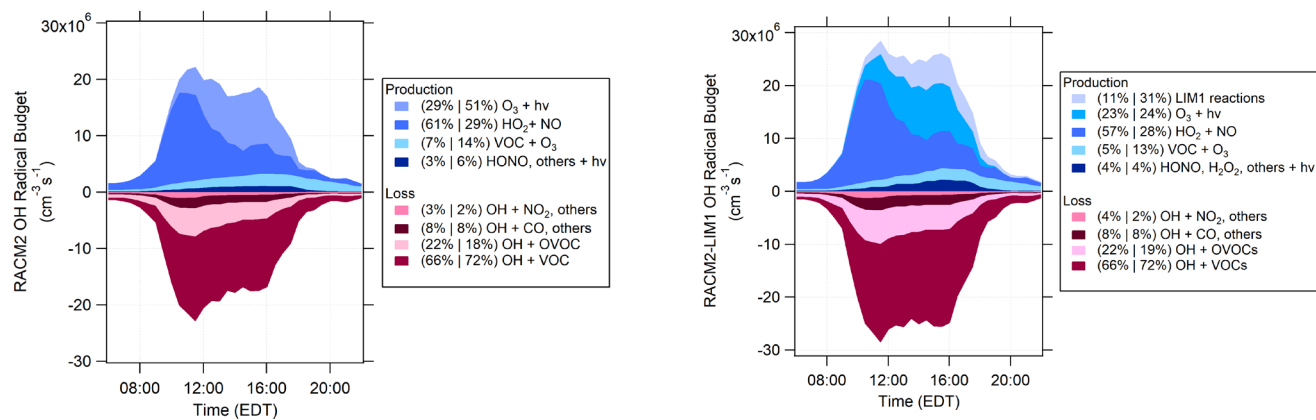
Figure 11. RACM2 (left) and RACM2-LIM1 (right) OH radical budgets where the shades of blue represent production reactions and the shades of red represent loss rates. The percent contribution of each reaction to total production/loss are divided into two periods (10:00 to 14:00 and 14:00 to 18:00).
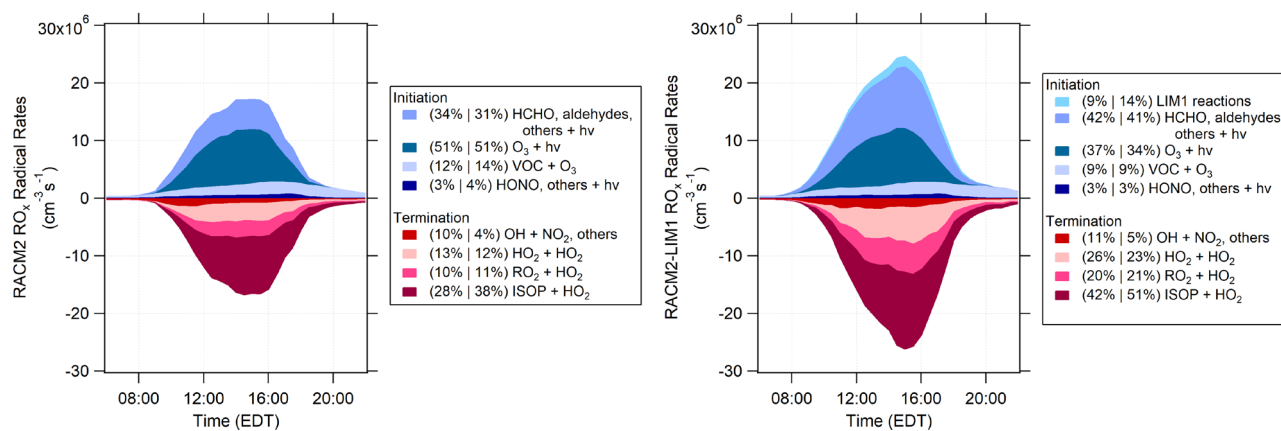
Figure 12. RACM2 (left) and RACM2-LIM1 (right) total RO_x radical budgets where the shades of blue represent initiation rates and the shades of red represent termination rates. The percent contribution of each reaction to total initiation/termination are divided into two periods (10:00 to 14:00 and 14:00 to 18:00).